Forestry: An International Journal of Forest Research, 2026, **99**, 1–20
https://doi.org/10.1093/forestry/cpaf087
Original Article

Evaluating RayCloudTools to estimate single-tree volume

Benjamin Wild[1,*], Taşkın Özkan[1], Moonis Ali[2], Florian Pöppl[1], Milutin Milenković[3], Florian Hofhansl[3], Norbert Pfeifer[1], Alvaro Lau[4], Markus Hollaus[1]

[1]Department of Geodesy and Geoinformation, TU Wien, Wiedner Hauptstraße 8, 1040 Vienna, Austria
[2]Department of Civil Engineering, Indian Institute of Technology Kanpur, Kanpur 208016, UP, India
[3]International Institute for Applied Systems Analysis (IIASA), Schlossplatz 1, 2361 Laxenburg, Austria
[4]Laboratory of Geo-Information Science and Remote Sensing, Wageningen University & Research, Droevendaalsesteeg 3, 6708 PB Wageningen, The Netherlands
[*]Corresponding author. Department of Geodesy and Geoinformation, TU Wien, Wiedner Hauptstraße 8, 1040 Vienna, Austria.
E-mail: benjamin.wild@geo.tuwien.ac.at

Abstract

Above-Ground Forest Biomass (AGB) is vital for understanding the carbon cycle, for carbon accounting, and for climate projections. Single-tree AGB measurements or precise estimates are crucial for calibrating and validating remote sensing based AGB mapping (e.g. in the area-based approaches), but remain costly and challenging to acquire. The recently introduced open-source RayCloudTools (RCT) software includes an efficient QSM (Quantitative Structure Model) solution, RCT-QSM that uses Dijkstra's algorithm to segment and volumetrically reconstruct trees, providing tree volume, which further requires density to obtain mass. The accuracy and practicability of RCT-QSM, however, have remained largely unassessed. This study provides a comprehensive evaluation of RCT-QSM, by comparing its volume estimates against: (i) three publicly available datasets of temporally coinciding TLS (Terrestrial Laser Scanning) scans and destructive measurements, (ii) four existing QSM methods (AdTree, TreeQSM, AdQSM, and SimpleForest), and (iii) allometric model outputs from two experimental plots in Austria, where point clouds were obtained with terrestrial and unmanned aerial vehicle (UAV)-based laser scanning. The comparison with destructively acquired single-tree data ($n = 124$) from three publicly available datasets shows an overall high correspondence between RCT-QSM derived volumes and destructively harvested volumes (CCC = 0.95) with a moderate negative bias (−7.3%) and an NRMSE of 5%. RCT-QSM outperforms other existing QSM solutions, such as AdTree, AdQSM, SimpleForest, and TreeQSM. TreeQSM metrics, however, show only small differences compared to RCT-QSM. An extensive point density sensitivity analysis featuring 1860 systematically downsampled point clouds from the same dataset demonstrates RCT-QSM's high robustness to variations in point density. Accuracy and completeness of the results remain stable for point densities as low as one point per 10x10x10 cm voxel. Regarding the large-scale applicability, RCT-QSM provides reliable results for two experimental plots in Austria, which were scanned with TLS and UAV-LS, respectively. RCT-QSM efficiently derives single-tree volume, aligning well with allometric models, demonstrating its applicability across various data acquisition settings and forest conditions.

Keywords: laser scanning; tree volume; QSM; allometry

Introduction

Above-Ground Biomass (AGB) is the total amount of dry plant biomass present above the ground. Since around 50% of dry plant biomass is carbon, AGB is a crucial variable for quantifying and understanding the global terrestrial carbon cycle (Le Toan et al. 2011) and other ecological functions such as temperature regulation (Arseniou et al. 2023). As such it has also been recognized as an Essential Climate Variable by various major international organizations (World Meteorological Organization et al. 2022) and is a key variable for the implementation of carbon accounting and climate projections (Stovall et al. 2018). Despite tremendous efforts in the field to improve AGB quantification approaches, the accurate and unbiased estimation of AGB, particularly in forests, continues to pose a substantial challenge at all spatial scales (Arseniou et al. 2023).

Globally, AGB and its dynamics are commonly estimated using satellite remote-sensing techniques that measure proxy variables (Tian et al. 2023) like Leaf Area Index, Canopy Height, and Vegetation Water Content in either the optical [e.g. Chopping et al. (2022), Fremout et al. (2022), Hirata et al. (2014), Hu et al. (2016)] or in the microwave domain [e.g. Huang et al. (2018), Schmidt et al. (2023), Teubner et al. (2021), Zotta et al. (2024)]. To obtain reliable estimates of AGB at a large-scale, satellite-based biomass products require reference data for calibration and validation. These data are typically collected in field campaigns during which tree parameters such as Tree Height (TH), Diameter at Breast Height (DBH), and tree species are determined. Using allometric models, single-tree volume can be calculated from these metrics. The single-tree volume can then be converted to AGB by multiplying it with a species-specific wood density, which can either be estimated experimentally *in situ* (i.e. through micro-drillings) or obtained from tabulated values such as the Global Wood Density Database (GWDD; Chave et al. 2009, Zanne et al. 2009).

In this context, allometric models have been a major research focus for decades, resulting in a substantial number of species-

Handling editor: Daniel Kükenbrink
Received 15 May 2025; **revised** 2 December 2025; **accepted** 5 December 2025

and biome-specific allometries. Many of them are publicly available in online databases such as GlobAllomeTree (globallometree.org; Henry et al. 2013) or in the form of scientific publications (e.g. by Zianis et al. 2005). Despite the great number of available allometric models, they are nevertheless limited by considerable variability in equations across different biomes and species (Dutcă 2019). Furthermore, large trees and urban trees are generally not well represented in most allometric equations due to their underrepresentation in the datasets used for model development (Stovall et al. 2018, Kükenbrink et al. 2021). This is not surprising as setting up accurate species and site-specific allometric models, usually involves destructive sampling of individual trees, which is not only time-consuming and expensive (Belete et al. 2021) but sometimes even dangerous and ethically questionable. Due to the typically limited number of destructively sampled trees and the natural variability of tree shapes, allometric equations have a limited transferability and accuracy. This introduces uncertainties that significantly contribute to the overall uncertainty in the biomass model development (Saarela et al. 2020).

Ground-based Laser Scanning (LS) has been identified as an independent, non-destructive remote sensing technology to quantify and derive single-tree volume (Ogle et al. 2019). Using a collection of 3D points, i.e. Point Clouds (PCs) obtained from LS, mostly from Terrestrial LS (TLS) or mobile LS (MLS), single-tree volumes can be derived with good accuracy using, e.g. quantitative structural models (QSMs; Fan et al. 2020; Hackenberg et al. 2015a; Raumonen et al. 2013). QSMs capture single tree structures by fitting cylinders to 3D points representing stem and branches. Integrating the volumes of fitted cylinders provides a direct estimate of the above-ground single-tree volume, which can be converted to AGB by multiplying it with the wood density (i.e. the ratio of dry mass to green volume; Swenson and Enquist 2007) of the measured tree. In recent years, the process of PC-based QSMs has been tested and applied extensively (e.g. Gonzalez de Tanago et al. 2018, Lau et al. 2018, Malhi et al. 2018, Momo Takoudjou et al. 2018, Stovall et al. 2018, Calders et al. 2020, Disney et al. 2020, Fan et al. 2020). Comparison with destructively harvested datasets collected across various biomes has proven that QSM-based volume estimates converted to AGB outperform allometric models derived from destructively harvested trees, thus making it an important resource especially when data from destructive harvesting is not available (Demol et al. 2022a).

While PC-based QSMs represent a promising avenue for estimating single-tree and plot-level volume they have also been shown to be prone to overestimating small branches. This particularly affects small trees (Demol et al. 2022b, Abegg et al. 2023), whose volume (and therefore AGB) consists largely of such branches. With increasing scanner-to-tree distance, branch volume was found to be severely overestimated (Morhart et al. 2024), indicating that established QSMs require tree-centered scan patterns (which are more time-intensive) to yield reliable results. While overestimation can be mitigated through careful planning and maintaining low TLS-to-tree distances, it restricts the applicability of PC-based QSMs for time-efficient, large-scale TLS campaigns and for LS data obtained from more efficient aerial platforms such as UAVs (unmanned aerial vehicles) or airplanes. Studies analyzing QSM-based volume estimation from UAV-LS have found very limited performance and significant overestimation of tree volume (Brede et al. 2019, Ye et al. 2019, Dalla Corte et al. 2022).

Recently a new, open-source PC-based approach for tree segmentation and volumetric reconstruction has been made available (Lowe and Stepanas 2021): The RayCloudTools (RCT) software toolbox. RCT implements various functions including a PC-based QSM algorithm referred to in this paper as RCT-QSM. This algorithm is freely available on GitHub (https://github.com/csiro-robotics/raycloudtools; (Lowe et al. 2021, Lowe and Stepanas 2021). So far, there are very few studies applying RCT-QSM for estimating single-tree volume. To the best of the authors' knowledge, as of October 2025, no published study has compared its performance against destructively harvested reference data. A recent study (Bohn Reckziegel et al. 2025) used RCT-QSM to derive woody volume and other forest characteristics from TLS and UAV-LS data. Their study showed that RCT-QSM enables volumetric reconstruction of single trees with a strong correspondence between volume measurements derived from TLS and UAV-LS. This highlights RCT-QSM's potential for efficiently estimating single-tree volume and consequently AGB on a large scale. Additionally, this study showed that leaf removal is not strictly necessary when using RCT-QSM, significantly reducing processing times compared to state-of-the-art QSMs. However, the authors also pointed out that more validation data, especially derived from destructively harvested single-trees, are needed to assess the applicability of RCT-QSM in operational workflows.

To this end, we investigate the accuracy and reliability of the RCT-based approach by comparing RCT-QSM single-tree volume with:

1) volumes from destructive sampling from three publicly available data sets,
2) volumes from four state-of-the-art QSM methods: AdTree (Du et al. 2019), TreeQSM (Raumonen et al. 2013), AdQSM (Fan et al. 2020), and SimpleForest (Hackenberg et al. 2015a), and
3) allometric model predictions for two experimental plots in Austria where TLS and UAV-LS data where acquired, respectively. This evaluates the reliability and robustness of RCT-QSM.

The secondary goal of this study is to test whether single-tree volume estimates obtained with RCT-QSM are sensitive to variations in point densities and how the algorithm works under more challenging acquisition conditions.

Data

Public datasets of coinciding destructive and terrestrial laser scanning measurements

The backbone of our validation of the RCT-QSM algorithm are three publicly available datasets of TLS scans of 130 trees, which were later destructively sampled. These trees originate from temperate and tropical forests in Belgium, China, Germany, Guyana, Indonesia, and Peru (Table 1). For the validation and comparison of RCT-QSM with four state-of-the-art QSM methods. In total six trees were excluded from the analysis: five from Demol et al. (2021a) and one from Gonzalez de Tanago et al. (2018). The trees from Demol et al. (2021a), all belonging to the species *Larix decidua*, were excluded due to reconstruction failures across the state-of-the-art methods, which can be explained with the species' characteristic low-branching structure, leading to unrealistic results for the state-of-the-art methods. RCT-QSM produced visually more realistic results. These data were nevertheless omitted from the analysis for better comparability. The tree from Gonzalez de Tanago et al. (2018) was excluded due to substantial gaps in the PC data along the trunk, which hindered accurate QSM reconstruction across all tested approaches.

Table 1. Overview of destructive datasets used in this study including site characteristics, PC acquisition settings and environmental conditions during scanning. n_t and n_s refer to the number of trees and species captured at each site.

Location	n_t	n_s	*Leave/needle conditions*	*Wind present*	*Scanner used*	*Number of scans per tree*	*Reference*
Germany	12	1	*Leaf-off*	*Yes*	*Z + F IMAGER 5010*	*6–8*	Hackenberg et al. (2015b)
China	24	2	*Leaf-on, needle-on*	*Yes*	*Z + F IMAGER 5010*	*6–8*	Hackenberg et al. (2015b)
Guyana	10	3	*Leaf-on*	*Not specified*	*RIEGL VZ-400*	*8–13*	Gonzalez de Tanago et al. (2018)
Indonesia	10	8	*Leaf-on*	*Not specified*	*RIEGL VZ-400*	*8–13*	Gonzalez de Tanago et al. (2018)
Peru	9	7	*Leaf-on*	*Not specified*	*RIEGL VZ-400*	*8–13*	Gonzalez de Tanago et al. (2018)
Belgium	65	4	*Leaf-off, needle-on and off*	*No*	*RIEGL VZ-400; VZ-1000*	*Scanned in a grid pattern with ca. 20 m grid width*	Demol et al. (2021b)

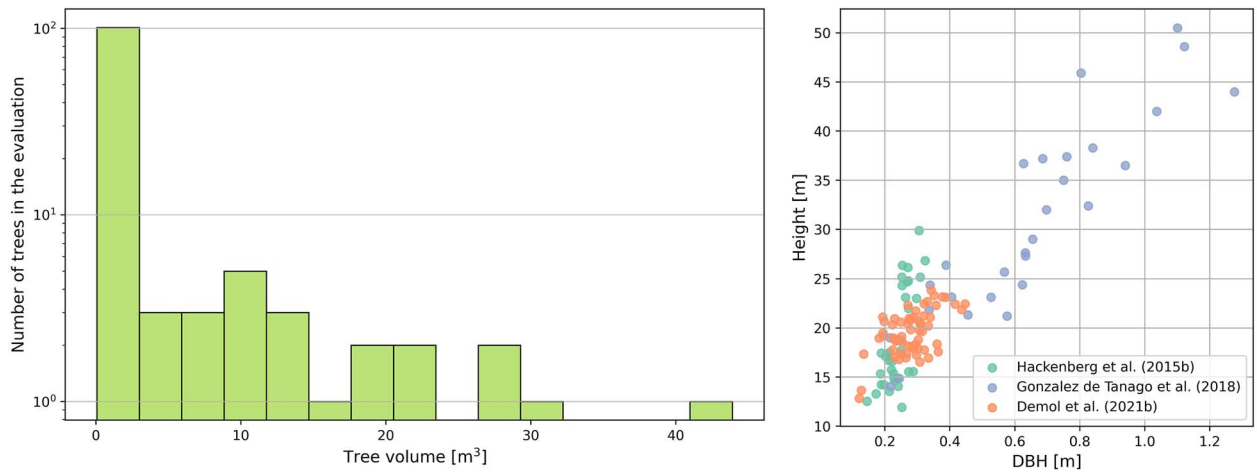

Figure 1. Tree volume distribution in m^3 as derived from destructive measurements (left) and scatterplot of DBH (in m, X-axis) and TH (in m, Y-axis) of the destructively harvested trees used in this study ($n = 124$, right).

The TLS scans were acquired with varying acquisition parameters and under distinct environmental conditions (Table 1). Data obtained in the Tropics from Gonzalez de Tanago et al. (2018) exhibit generally more occlusions in the upper canopy than those obtained from Demol et al. (2021b) or Hackenberg et al. (2015b). The datasets offer a large variety (Fig. 1) in terms of tree size and species distribution. DBH values range from 11.5 cm to 127.6 cm with heights between 12.6 m and 50.5 m. Regarding the volume distribution, most trees are below 10 m^3, with some individual trees from the tropical dataset substantially exceeding these values.

The methodologies for estimating single-tree volumes differ between datasets. Gonzalez de Tanago et al. (2018) determined volume directly by measuring stem and branch diameters at 1-meter intervals along the stem and branches, focusing on branches exceeding a 10 cm diameter threshold. In contrast, the other campaigns first measured the "green" or "fresh" mass of the trees by weighing them immediately after harvest. Hackenberg et al. (2015b) and Demol et al. (2021b) included in their measurement smaller branches within diameter classes of 2.5–10 cm, while excluding branches below 2.5 cm. From the derived green mass, the dry mass (i.e. AGB) was calculated using the dry matter content, defined as the ratio of dry mass to green mass. The derived AGB was then converted to volume by dividing it by the species-specific wood density, which is the ratio of oven-dry mass to green volume. These conversions introduce some uncertainties, as discussed in Section 5.

Terrestrial laser scanning, unmanned aerial vehicle-laser scanning, and allometric data obtained at two experimental plots

In addition to the destructively harvested reference data, the validity and scalability of RCT-based segmentation and RCT-QSM were further evaluated using data from two experimental plots in Austria (Table 2, Figs 3 and 4). Since destructive reference data were unavailable for these plots, well-calibrated genus-specific allometric models served as the primary reference. At experimental plot A, a standard multistation TLS procedure was employed. At Site B, UAV-LS data were collected to test RCT-QSM under more challenging, dynamic acquisition conditions. These approaches provide additional insights into RCT-QSM's applicability across varying scenarios. The following sections describe the two experimental plots and associated data acquisition methods in detail.

Experimental plot A

Experimental plot A is located in Prater, a recreational area in Vienna. The area within Prater that was selected for this study is a mildly managed forested area of ca. 3000 m^2 with little understory

Table 2. Summary of key characteristics of experimental plot A and B and the corresponding LS campaigns.

Experimental plot	*A*	*B*
Location	*Prater, Vienna, Austria*	*Rohrach, Vorarlberg, Austria*
FAO Biome	*Temperate continental forest*	*Temperate mountain forest*
Sample Area [m^2]	*3000*	*1300*
Number of trees used for validation	*110*	*19*
DBH range of samples [cm]	*[10.0, 76.7]*	*[16.4, 75.1]*
Tree Height range of samples [m]	*[8.2, 27.7]*	*[8.4, 41.8]*
Dominant Genera	*Maple (Acer)*	*Beech (Fagus), Spruce (Picea)*
Laser Scanner	*RIEGL VZ-600i*	*RIEGL VUX-120*
Camera	*Sony α7R IV*	*PhaseOne iXM100*
Platform	*Tripod, ground-based*	*UAV, airborne*
Scanning date	*03–2024*	*04–2022*
Leaf/Needle conditions	*Leaf-off*	*Leaf-off, Needle-on*

(Fig. 2C). For the TLS campaign, a *RIEGL* VZ-600i was used. The scanner has a beam divergence of 3.5 mrad, which corresponds to a beam diameter increase of 3.5 cm per 100 m. The 3D point accuracy is documented as 3 mm at 50 m and 5 mm at 100 m. A pulse repetition rate of 2200 kHz was used, with an angular spacing of 0.034°. The scanning data was acquired just before the onset of foliage in early spring. During the TLS campaign little to no wind was present. The scanning conditions can thus be summarized as favorable for tree volume estimation.

Experimental plot B

Experimental plot B is in the Rohrach forest in Vorarlberg, Austria (Fig. 3). It is classified as natural forest reserve (German: *Naturwaldreservat*) with minimal human influences (Grabherr et al. 1999). The entire forest was surveyed in April 2022, prior to the onset of foliage but with needles present on evergreen trees. Data collection utilized a *RIEGL* VUX-120 laser scanner (*RIEGL* Laser Measurement Systems GmbH, Horn, Austria) and a PhaseOne iXM100 camera mounted on an UAV. The flying height over ground was ∼160 m. The RIEGL VUX-120 employs a nadir-forward-backward scanning pattern and has a nominal ranging precision of 5 mm.

Tree parameter estimation as input for allometric models

Species-specific allometric models require single-tree parameters such as DBH and TH as input to derive single-tree volume or AGB. At experimental plot A, where TLS data was acquired, DBH was automatically derived using two software tools: 3DFIN (Laino et al. 2024) and OPALS (Pfeifer et al. 2014). Both tools provide key tree parameters, including DBH, TH, and tree positions. For this analysis, only trees with a DBH > 10 cm were considered. Tree positions were used to align and compare outputs from the two solutions via nearest neighbor matching. If DBH values from the two solutions differed by <1 cm, the results were considered reliable. This was verified by randomly checking a subsample of trees. For cases with significant discrepancies, the affected trees were manually remeasured in the PC using the measurement tool in CloudCompare (Girardeau-Montaut 2024). This additional step ensured high accuracy and preserved data integrity.

Experimental plot A is predominantly composed of trees from the genus maple (*Acer*). Individuals from other genera were present only sporadically and were excluded from the present analysis, which resulted in 110 trees studied in plot A. Among the genus *Acer*, three species were identified on-site: Sycamore maple (*Acer pseudoplatanus*), Norway maple (*Acer platanoides*), and Sugar maple (*Acer saccharum*). However, due to the lack of adequate biome-specific allometric models for Sycamore maple and Norway maple, all trees were modeled using allometric equations for Sugar maple. This decision was based on the availability of several well-constrained models for Sugar maple (Table 3) under comparable climatic conditions (FAO biome: "temperate continental forest") and the assumption that inter-genus differences are small. This approach was considered the most robust and reliable means of obtaining independent reference AGB values for many trees. Moreover, AGB is frequently estimated using broadly generalized, non-species-specific models (e.g. Chave et al. 2005). The various allometric (Table 2 and 3) AGB estimates for "Acer" trees from experimental plot A were averaged and converted to volume by dividing the results by the species-specific basic wood density of *A. saccharum* (560 kg/m^3), as listed in the GWDD (Chave et al. 2009, Zanne et al. 2009).

At experimental plot B, automated parameter extraction was unsuccessful, presumably due to the low point density especially along the lower sections of the trunk. Instead, DBH and TH were manually measured for trees that were sufficiently well reconstructed in the PC. Manual DBH measurements proved particularly challenging due to significant PC gaps along the tree stems. To ensure integrity of the results, trees for which DBH could not be retrieved unambiguously as well as very small trees (DBH < 10 cm) were excluded from the analysis. As a result, the number of trees analyzed was reduced from 40 to 19. On-site species identification was not possible at experimental plot B. Instead, tree species were classified using imagery collected by the UAV (Fig. 3C). A true orthophoto with a Ground Sampling Distance of ∼2 cm was generated from the imagery and used for visual species identification. Trees with ambiguous identification were excluded from further analysis. Of the remaining 19 trees, 14 were identified as European beech (*Fagus sylvatica*) and five as Norway spruce (*Picea abies*). Reference volumes for these trees were obtained using the species-specific allometric models and parameters detailed in Tables 3 and 4.

Methods

RayCloudTools

In this study the open-source RCT toolbox (Lowe and Stepanas 2021), developed by Commonwealth Scientific and Industrial Research Organization, was utilized to process the LS data. For a detailed explanation of the methodology, readers are referred to Lowe and Stepanas (2021). The following provides a summary of the key methodology implemented in RCT, with

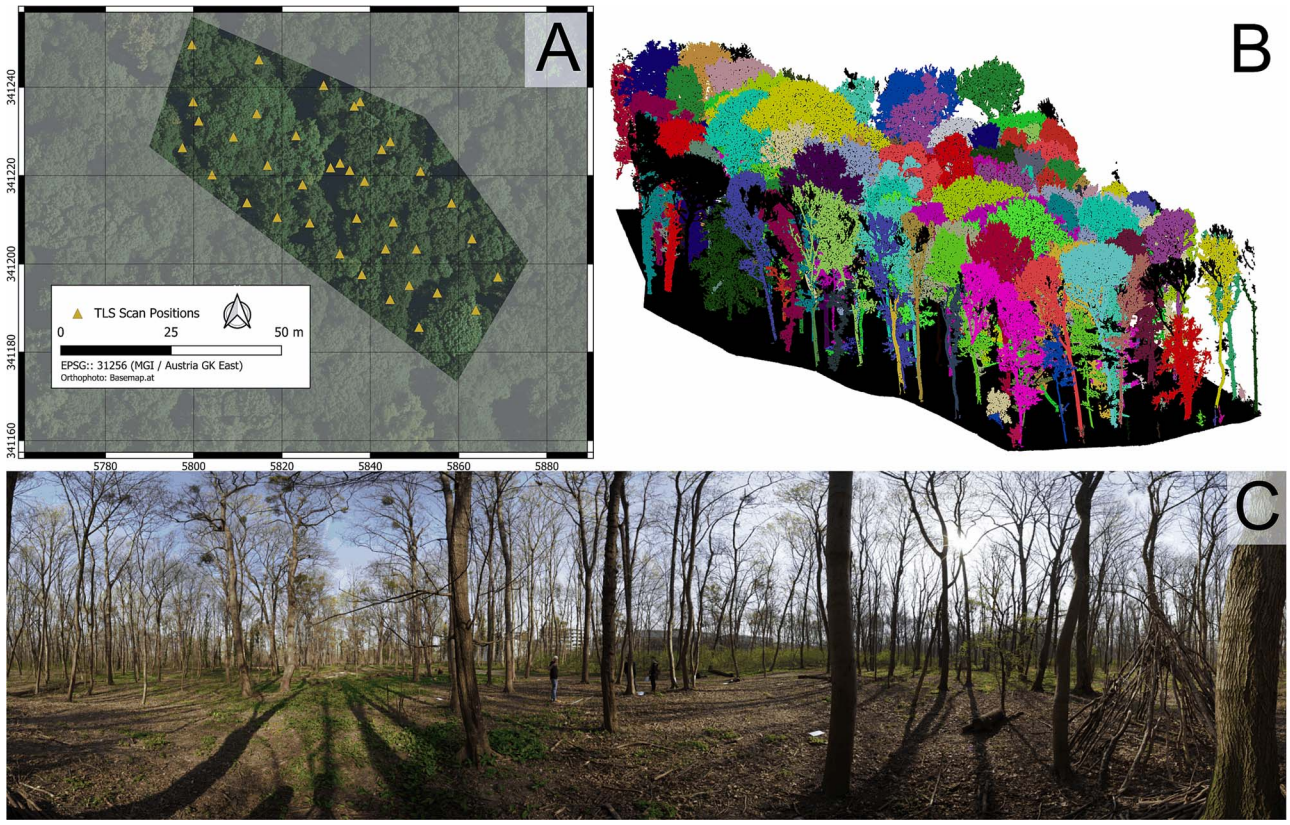

Figure 2. (A) Orthophoto showing the approximate boundaries of experimental plot A. (B) Segmented PC of experimental plot A, generated using RCT. (C) Panoramic 360-degree image from a scan position within experimental plot A.

Table 3. Species-specific allometric models used for AGB and volume retrieval. The empirically derived coefficients of the respective model can be found in Table 3.

Species	*Allometric model*	*Units*	*Reference*
Sugar maple	$AGB = a * DBH^b$	*AGB in kg; DBH in cm*	Ter-Mikaelian and Korzukhin (1997)
European beech	$Volume = \frac{\pi}{4} * \left(a * DBH^2 * TH - b * DBH^2 + c * DBH\right)$	*Volume in dm^3 DBH and TH in dm*	Schieler (1988)
Norway spruce	$Volume = \frac{\pi}{4} * \left(a * DBH^2 * TH - \left(b * DBH^2 * TH * Log^2(DBH)\right) - \left(c * DBH^2\right) + d * DBH\right)$	*Volume in dm^3 DBH and TH in dm*	Schieler (1988)

Table 4. Empirically derived and published coefficients of the allometric models from Table 2.

Species	*Used for experimental plot*	*a*	*b*	*c*	*d*	*FAO Biome*	*N*	R^2	*Reference*
Sugar maple	A	0.2064	2.33			TCF	5	0.998	Bickelhaupt et al. (1973)
	A	0.1252	2.48			TCF	5	0.984	Bickelhaupt et al. (1973)
	A	0.1008	2.57			TCF	119	0.980	Brenneman et al. (1978)
	A	0.1532	2.39			TCF	36	0.995	Freedman et al. (1982)
	A	0.1599	2.34			TCF	45	0.993	Ker (1980)
	A	0.1259	2.36			TCF	9	0.99	Pastor and Bockheim (1981)
	A	0.1676	2.36			TCF	42	*n.a.*	Perala and Alban (1994)
	A	0.1641	2.42			TCF	14	0.998	Whittaker et al. (1974)
	A	0.1891	2.33			TCF	42	*n.a.*	Young et al. (1980)
Norway spruce	B	0.563443	0.12731	8.55022	7.6331	TMS	*n.a.*	0.81	Schieler (1988)
European beech	B	0.5173	13.62144	9.9888		TCF	*n.a.*	0.75	Schieler (1988)

N refers to the number of destructively harvested trees that were used by the respective reference for the parameter retrieval and R^2 indicates the goodness of fit for the respective model. TCF corresponds to FAO Biome "Temperate Continental Forest" and TMS corresponds to "Temperate Mountain System".

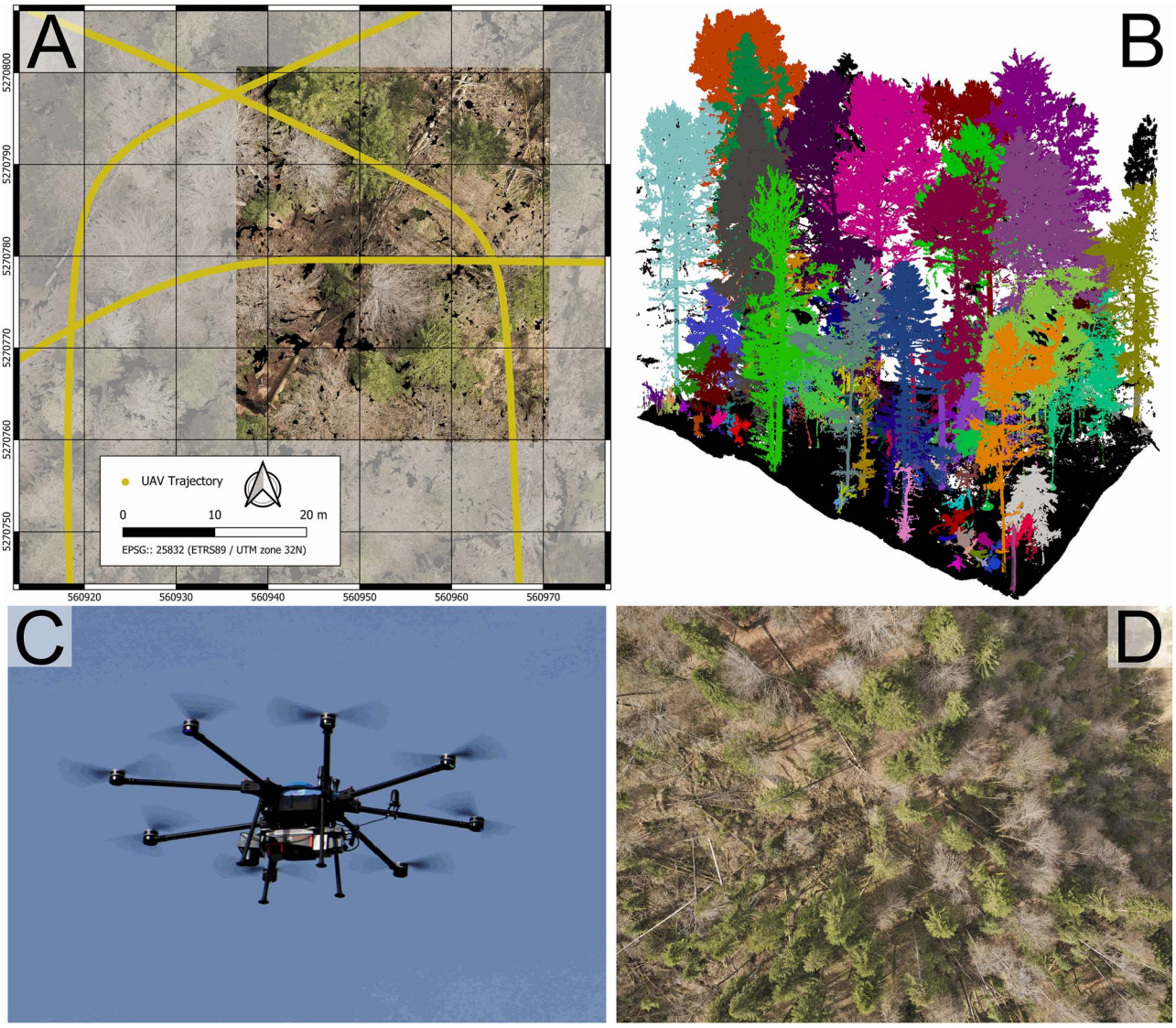

Figure 3. (A) Orthophoto of the experimental block B showing the trajectory (yellow line) of the UAV-LS. (C) The UAV-LS during operation at the experimental plot. (B) Segmented PC of experimental plot B generated using RCT. (D) Aerial image of the surveyed forest obtained from the PhaseOne iXM100 camera mounted on the UAV.

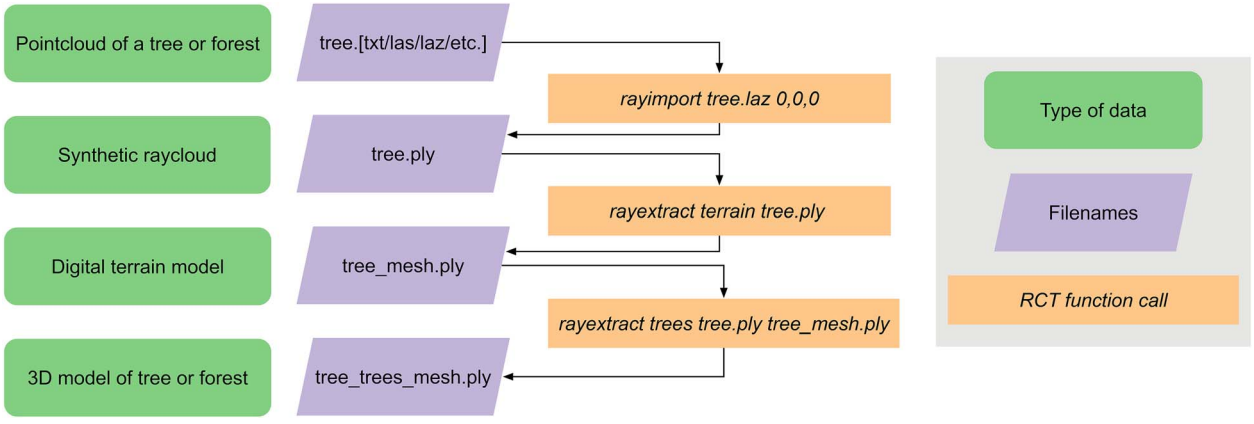

Figure 4. Workflow diagram of the main RCT processing steps and the corresponding type and format of the respective input and output data.

a particular emphasis on RCT-QSM. Readers are encouraged to consult the GitHub repository (https://github.com/csiro-robotics/raycloudtools) for the most current information and updates. For this evaluation, the latest publicly available version of RCT at time of processing (14 November 2024, with commit hash 9f696d0) was utilized.

Deriving a QSM from a PC using RCT involves a multistep processing workflow (Fig. 4). The process starts by converting the PC, which may contain multiple trees, into a (synthetic) ray-cloud file, which includes the vector from each LS point to the sensor's position during measurement, enabling the reconstruction of the individual ray-vectors (from endpoint to source). While RCT, as the name suggests, is fundamentally based on the ray-cloud concept (Lowe and Stepanas 2021), its default RCT-QSM does not use this ray information. Only a recently introduced "use-rays" option allows incorporating sensor positions to reduce overestimation of trunk diameters in noisy datasets. However, after personal communication with one of the developers, this study excluded the option for two reasons: (i) its impact is minimal for low-noise PCs, and (ii) it requires TLS scan positions or trajectory estimates, which are not publicly available for the destructive datasets used here. To meet RCT's requirement for ray-cloud file fields, a synthetic ray-cloud was generated by assigning an arbitrary, static ray origin (e.g. 0, 0, 0).

This synthetic ray-cloud is then used to derive a digital terrain model employing a so-called visibility culling technique (Katz and Tal 2015). This approach involves modifying the vertical component of the points by adding a paraboloidal function. A convex hull is then computed from these modified points using qhull (http://www.qhull.org/), generating an indexed mesh. The upper surface of the convex hull is removed, leaving a mesh that approximates the lower bound of the terrain surface. Finally, the paraboloidal function is subtracted, yielding a triangle mesh that serves as an approximation of the ground surface (Lowe et al. 2021).

This mesh, together with the synthetic ray-cloud, serves as input for RCT-QSM, implemented in the "rayextract trees" function, which segments and reconstructs trees using Dijkstra's shortest path algorithm. This results in a forest of disjoint acyclic graphs, where each point is linked to a nearby parent. To trace the branches, the edge lengths in the graph are determined using squared distances rather than the standard Euclidean distance. Additionally, these edge lengths are weighed to penalize large direction changes from root to leaf. The shortest paths with the longest Euclidean distances are clustered to identify the root points of each tree stem. From these roots, the tree's structure is iteratively computed, segment-by-segment, as cylindrical shapes. New branches are formed whenever a child point significantly deviates from the stem (Bohn Reckziegel et al. 2025). It is to be noted here, that besides the "use-rays" parameters there are other parameters, such as a maximum distance between neighboring points in a tree, which can be specified in RCT-QSM. In this study the sensitivity of these parameters to the results was not assessed but instead the default values were used.

The derivation of single-tree volumes from the generated RCT-QSMs was automated using a custom python script which computes the volume of each generated mesh-file using the open-source library PyMeshLab (https://github.com/cnr-isti-vclab/PyMeshLab, last accessed: 12 December 2024; Muntoni and Cignoni 2021).

State-of-the-art quantitative structural model algorithms used for comparison

To evaluate and contextualize the performance of RCT-QSM, a comparative analysis was carried out against volumetric reconstruction obtained from four state-of-the-art QSM algorithms. The comparison includes AdTree (Du et al. 2019), TreeQSM (Raumonen et al. 2013), AdQSM (Fan et al. 2020), and SimpleForest (Hackenberg et al. 2015a). The volume reconstructions produced by these algorithms were initially conducted and published by Ali et al. (2025). The following summaries are adapted from their study and provide a concise overview of how each QSM was derived using the respective methods.

TreeQSM

TreeQSM, introduced by Raumonen et al. (2013), reconstructs trees by fitting hierarchically organized cylinders to the tree's surface derived from TLS PCs. The method starts with noise filtering and PC segmentation into connected surface patches. These patches are assembled using a building-brick strategy and later segmented into nested cylinders representing branches and stems. In this study, TreeQSM version 2.4.1 was used due to its more reliable handling of small branches compared to later versions. The algorithm, implemented in MATLAB, allows for extensive parameter tuning. The parameters *PatchDiam1*, *PatchDiam2Min*, and *PatchDiam2Max* were optimized across various geographical locations to ensure robust modeling. Optimized parameter values were chosen from three tested combinations of the parameters for 20% of the destructively harvested trees as sample trees, balancing accuracy and computational cost. The eventually determined parameters for *PatchDiam1*, *PatchDiam2Min*, and *PatchDiam2Max* were 2, 4, and 3.

SimpleForest

SimpleForest is an extension of the SimpleTree framework (Hackenberg et al. 2015a, 2015b), offering advanced pre-processing routines including outlier removal, voxel grid filtering, and curvature filtering. Tree reconstruction uses a PCA-based stem detection and the "SphereFollowing method" for cylinder fitting. Implemented as a plugin in CompuTree, SimpleForest allows for considerable customization, including automatic optimization of three core parameters across 125 combinations. Post-fitting, a median filter is applied to correct irregularities, and the "SphereFollowing Advanced" algorithm is used to refine fitting by cluster (e.g. stem vs. branches). Despite offering additional filtering options, such as shoot correction, these were omitted here due to their tendency to introduce inaccuracies in cylinder diameter. This decision was based on empirical observations from our dataset, where these filters consistently produced underestimated measurements. As a result, maintaining geometric fidelity took precedence over theoretical corrections.

AdTree and AdQSM

AdTree (Du et al. 2019) employs a fully automated pipeline for generating detailed 3D tree models from PCs. It begins with skeleton extraction using Delaunay triangulation and MST analysis, followed by simplification and cylinder fitting to model the main trunk and branches. Although AdTree does not perform geometric analysis (e.g. volume estimation), the model can be converted into a watertight mesh in CloudCompare, where the volume is computed using the "Measure Volume" function.

AdQSM (Fan et al. 2020) builds on AdTree by introducing semi-automated trunk identification and direct volume estimation. It uses the same MST-based skeleton extraction but requires manual input to ensure accurate trunk fitting. Two critical parameters, Height Segmentation (HS) and Cloud Parameter, govern model accuracy. Volume estimates are averaged across a range of parameter settings to enhance reliability. AdQSM offers a more streamlined workflow with minimal parameter tuning, making it a practical alternative to more complex QSM frameworks, particularly for large-scale or time-sensitive applications.

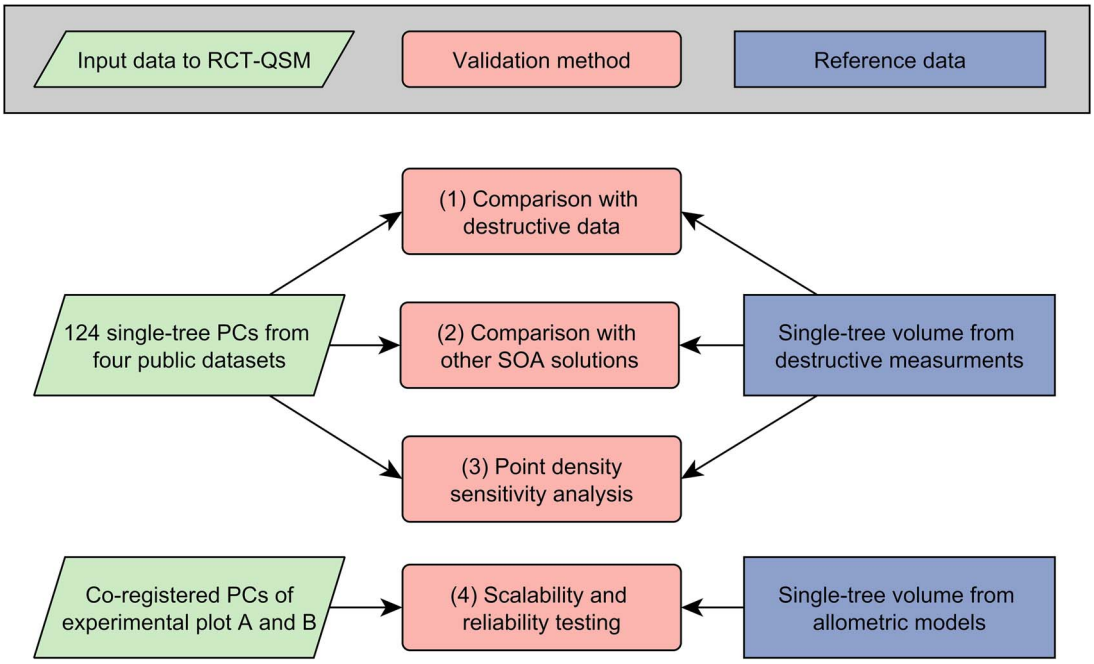

Figure 5. Diagram displaying the methodological framework including the respective input data for RCT-QSM and the used reference data.

Validation framework

To evaluate the performance and applicability of RCT-QSM, this study employs the following methodological framework (Fig. 5):

(1) **Comparison with destructive sampling:** RCT-QSM results were qualitatively and quantitatively compared to destructively determined single-tree volume and AGB measurements from the previously introduced 124 trees. The metrics used in this comparison are detailed in Section 3.3.2.

(2) **Comparison with other state-of-the-art QSM solutions:** The results from RCT-QSM were validated against results obtained from four state-of-the-art QSM algorithms. These include AdTree (Du et al. 2019), TreeQSM (Raumonen et al. 2013), AdQSM (Fan et al. 2020) and SimpleForest (Hackenberg et al. 2015a).

(3) **Point density sensitivity analysis:** The PCs used in the destructive sampling evaluation were systematically downsampled. The downsampling yielded point densities of 1 point per 0.1 cm voxel to 1 point per 50 cm voxel. RCT-QSM models were generated for each density level. The obtained results were compared against the destructive reference data. This analysis provides insights into how point density affects reconstruction accuracy and runtime and is detailed in Section 3.3.1. For comparison, volumes and runtime for model generation as functions of point density were also analyzed for TreeQSM, which has proven to be the best of the state-of-the-art methods.

(4) **Scalability and reliability testing:** Single-tree volumes derived from allometric models at experimental plots A and B were compared to RCT-QSM estimates using the same metrics as in (1). In contrast to (1), (2) and (3), the input data for this analysis are not presegmented PCs of single-trees but one co-registered PC for the experimental plots A and B, respectively. This evaluation assesses the method's scalability in terms of accuracy and computational requirements.

All computations using RCT-QSM were executed on an Intel(R) Xeon(R) CPU E5-2650 v4 @ 2.20GHz with 512 GB of RAM.

Point density sensitivity analysis

A systematic sensitivity analysis was performed to evaluate how changes in point density affect RCT-QSM. The ray-cloud for each of the 124 trees was systematically downsampled using RCT's "raydecimate" function, which spatially reduces the density of points to one point per x cm voxel, by picking one point within each voxel (Lowe and Stepanas 2021). Fifteen resampling parameters were tested: 0.1, 0.5, 1, 2, 3, 4, 5, 7, 8, 9, 10, 15, 20, 30, and 50 cm voxel size. This resulted in a total of 1860 PCs (15 parameters × 124 trees), which were processed using the processing chain depicted in Fig. 4. For consistency, the same ground mesh, derived from the original PC, was applied across all reconstructions, assuming that in real-world scenarios, a sufficiently accurate ground mesh can be obtained. Differences in the resulting volumetric reconstructions were visually inspected, and a detailed numerical sensitivity analysis was carried out using the metrics described in Section 3.3.2.

Statistical evaluation

The RCT-QSM-derived volumes from the various scenarios as well as the volumes reconstructed using state-of-the-art QSMs were compared with the respective reference volumes, which were obtained either through destructive sampling, or modeled using allometric equations. This comparison was performed qualitatively by visually inspecting and analyzing the reconstructed models and quantitatively through linear regression analysis and the computation of the following performance metrics: relative bias, concordance correlation coefficient (CCC; Lin 1989), Root Mean Square Error (RMSE), and Normalized Root Mean Square Error (NRMSE), which is normalized by dividing the RMSE with the absolute difference between maximum and minimum of the reference values.

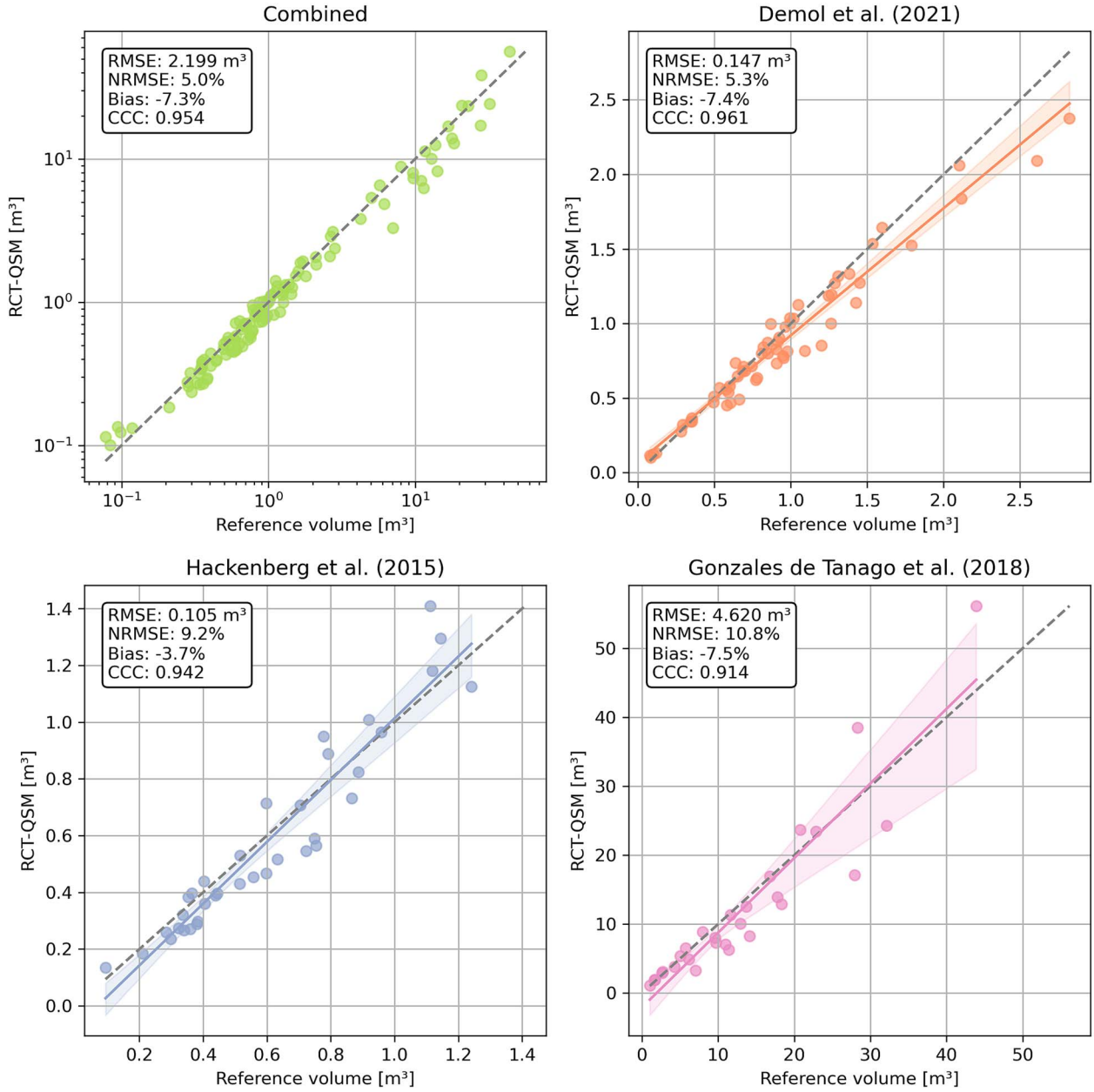

Figure 6. Comparison of destructively measured volumes with RCT-QSM-derived volumes across all datasets (upper-left) and for individual datasets. The upper-left plot uses logarithmic scaling for the axes to accommodate the wide range of single-tree volumes, while the individual dataset plots feature linear scaling with axis limits tailored to each dataset. Shaded regions around the linear regression lines represent the 95% confidence intervals of the corresponding regression models. The dashed line corresponds to the 1:1 reference line.

Results and discussion

Comparison with destructive data

In the combined analysis featuring all 124 trees (Fig. 6), the CCC between RCT-QSM and reference volume is 0.954, with a small but consistent negative bias, which can be observed across all datasets investigated. The bias is less pronounced for Hackenberg et al. (−3.7%) than for Demol et al. (−7.4%) and Gonzales de Tanago et al. (−7.5%). Overall accuracy, expressed as NRMSE, is highest for the dataset by Demol et al. (5.3%, $n = 60$) and slightly worse for Hackenberg et al. (9.2%, $n = 36$) and Gonzales de Tanago et al. (10.8%, $n = 28$). No clear pattern (species distribution, PC characteristics, etc.) was found to further explain those differences. The computed linear regressions align closely with the plotted 1:1 reference lines.

Comparison with other state-of-the-art quantitative structure model solutions

A comparison of RCT-QSM with several state-of-the-art methods, including AdQSM, TreeQSM, AdTree, and SimpleForest, reveals that RCT-QSM and TreeQSM deliver the best overall performance (Figs 7 and 8). For each tool we followed the suggestions of authors and developers for achieving best results. The performance differences between RCT-QSM and TreeQSM are minimal. While TreeQSM achieves slightly lower RMSE and NRMSE values, RCT-QSM demonstrates marginally superior performance in terms of CCC and bias. In contrast, AdQSM and SimpleForest exhibit substantial systematic biases of −30.3% and 21.9%, respectively. With respect to (N)RMSE, AdQSM, AdTree, and SimpleForest show comparable errors around 7%, approximately 2 percentage points

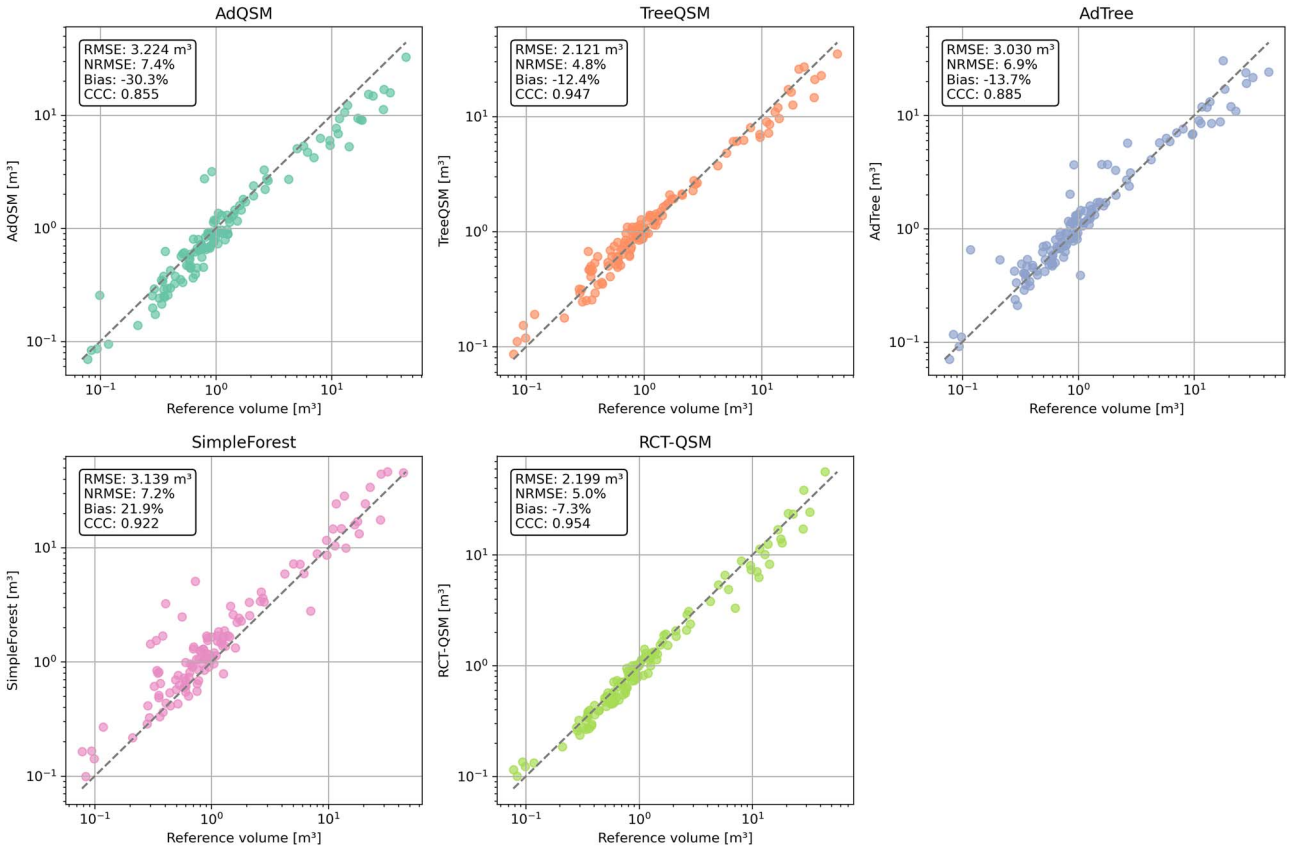

Figure 7. Comparison of destructively measured tree volumes with volumes obtained from the five tested state-of-the-art QSM algorithms AdQSM, TreeQSM, AdTree, Simple Forest and RCT-QSM.

higher than those of RCT-QSM and TreeQSM. These results collectively indicate that TreeQSM and RCT-QSM are the most accurate and reliable methods among those evaluated. The RCT-QSM processing time for a single pre-segmented PC is on the order of 5 s, depending on the size of the input PC.

An exemplary visual analysis of two relatively large tropical trees from Gonzales de Tanago et al. (IND10 and GUY01; Fig. 9, Table 5) exhibits differences between the reconstruction results. RCT-QSM demonstrates the most detailed reconstruction result, modelling very fine branches in the upper tree crown. For GUY01, which has point coverage throughout the canopy, these fine-scale RCT-QSM reconstructions appear largely realistic upon closer inspection. In contrast, some small branches in IND10 appear artificially inferred. Here it should be noted that the software "treetools" (Lowe et al. 2021) offers manipulation of RCT-QSM derived results offering also a pruning function which allows pruning branches larger than a certain diameter. For this analysis no pruning was applied. Despite accurately reconstructing the tree crown, RCT-QSM, like other QSM methods except AdTree, significantly underestimated the volume of GUY01. This is primarily due to a consistent underestimation of lower stem diameters, and particularly a severe underestimation of buttresses. Such issues are known for QSM applications and often result in systematic underestimation of tropical trees, where buttresses can contain a substantial proportion of AGB (Ali et al. 2025).

Despite a substantially lower point density beginning in the upper half of IND10's trunk, all reconstructions are largely complete, in the sense that no large tree parts are missing in its reconstruction or in that of any other tree. SimpleForest reconstructs few higher-order branches and twigs, yet yields the highest volume, affirming that accurate trunk reconstruction is the primary driver for high-quality QSM volume estimates. TreeQSM exhibits partly unrealistic tree volume in the upper canopy for IND10. Despite the presence of some inaccurate model components, the total volume closely aligns with the reference volume. Given the large sample size used in this comparative analysis, the results presented in Figs 7 and 8 can be considered robust. However, Fig. 9 serves as a reminder that, for individual trees, QSM may occasionally produce accurate tree-level volume estimates for the wrong reasons. Future studies could benefit from a more detailed assessment of QSM accuracy across distinct tree compartments.

Point density sensitivity analysis

PCs with decreasing density were generated by thinning out the original PC. At the levels of voxel sizes 0.1, 0.5, and 1 cm practically no notable change in the total number of points per tree occurred: median point number per tree drops from 355 000 to 339 000 points. When changing the voxel size from 2 cm to 10 cm, the point number is reduced considerably and the median drops from 174 000 to 16 000 points (i.e. one order of magnitude). For the lowest density of 1 point per 50 cm voxel the median point number is 780.

The sensitivity analysis reveals a strong relationship between PC density and the robustness of RCT-QSM reconstructions. The method maintained high reconstruction success rates down to a density of 1 point per 10 cm voxel, with 98% of PCs yielding valid QSMs. However, a sharp decline in success was observed below this threshold, dropping to ~52% at 1 point per 20 cm voxel and just 15% at 1 point per 50 cm voxel (Figs 10a, and 11,

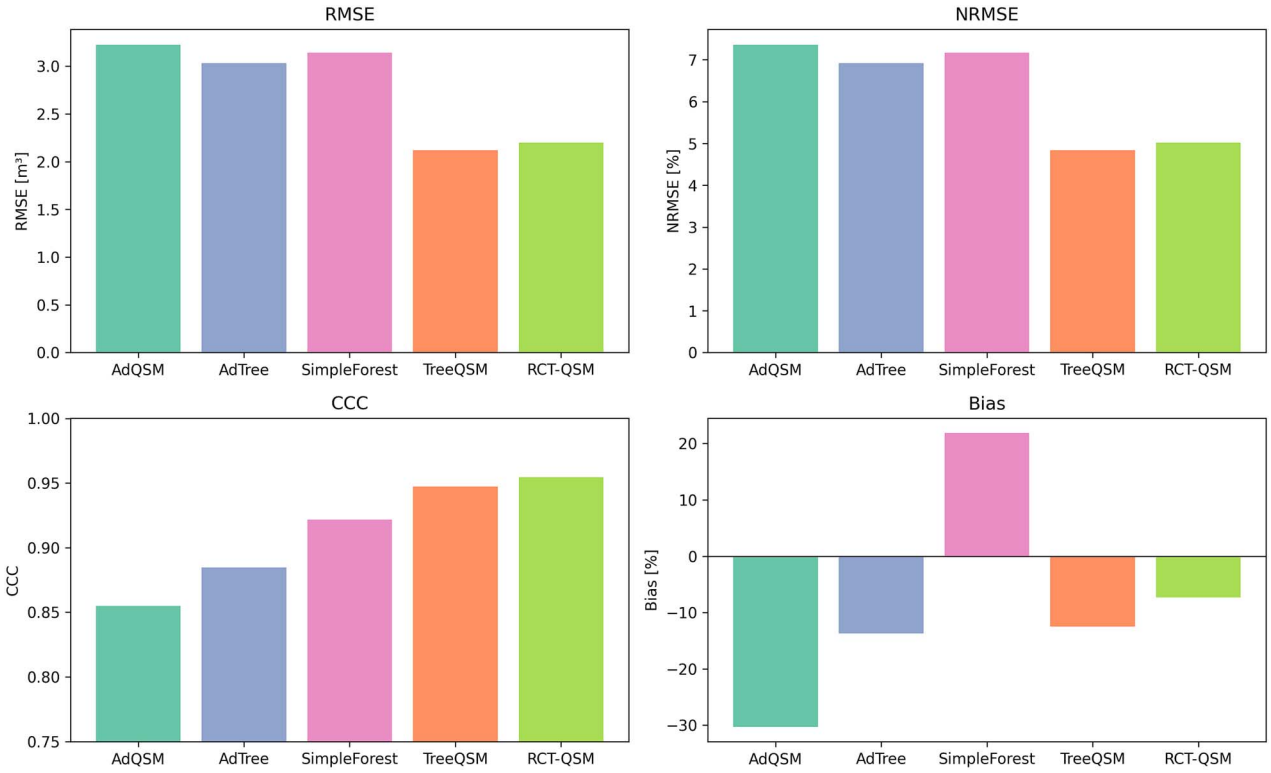

Figure 8. Bar plots showing the obtained error metrics for the five tested solutions ($n = 124$).

Table 5. Numerical results for the trees presented in Fig. 9.

Tree ID	*Reference volume [m^3]*	*RCT-QSM [m^3]*	*AdQSM [m^3]*	*AdTree [m^3]*	*SimpleForest [m^3]*	*TreeQSM [m^3]*
GUY01	18.32	12.89	9.02	17.06	13.25	12.57
IND10	2.74	3.09	2.76	2.38	3.63	2.58

RCT-QSM curves in green). When considering only successful reconstructions, error metrics such as bias, CCC, and (N)RMSE did not exhibit a clear dependence on point density, but substantial variability of the metrics was observed across different resampling configurations (Figs 11 and 12). This trend is consistent with visual assessments of reconstructed trees (Fig. 13), which showed no clear improvement in structural accuracy at higher point densities. These findings suggest that, when RCT-QSM produces a reconstruction, it can generally be considered reliable. However, it is important to note that the analysis was based on high-quality PCs acquired using advanced scanners and dense scanning protocols. For PCs with higher noise levels or uneven sampling, the influence of point density is expected to be more significant.

There is, however, a notable effect of point density on runtime. On the processing machine used (see Section 4.4.1 for details), the median runtime remained stable at 7 s per tree, even when the PC was thinned up to a density of 1 point per 2 cm voxel. Decreasing density further to 1 point per 10 cm voxel, there is a slight drop from 7 to 3 s per tree. This goes along with a median point reduction to 5% of the original number. For sparser PCs runtime decreases strongly, but—as shown above—also quality of volume estimates does. There is, however, a notable variation in runtime per tree, at full resolution this ranges between 0.7 and 101 s, which is attributed to the variety in the different public data sets. As can be expected, a larger number of points corresponds to larger processing times, but the correlation is around 50% only (R^2 value).

This analysis was also performed for TreeQSM, since Section 4.2 showed that its performance was very similar to that of RCT-QSM and exceeded that of the other QSM algorithms. For each density, optimization of the parameters was performed based on the distance RMSE between the PC and the fitted model. Lowering resolution leads to increasing errors, but up to a density of 1 point per 3 cm voxel the errors increase in size comparable to the errors of RCT-QSM, albeit with a bigger variation (see Figs 10b, 11, and 12). For lower density up to 1 point per 5 cm voxel the errors and variation increase, most notable is the increase in bias. However, the errors metrics are comparable in magnitude to those of RCT-QSM. For even sparser PCs, the errors metrics grow strongly, suggesting a nonlinear increase in error in relation to reference volume. Up to a density of 1 point per 10 cm voxels models are generated for all trees, but for lower density no models are generated. Runtime behavior of TreeQSM across different densities is similar to RCT-QSM and also in the same order of magnitude. Results on runtime are not directly comparable on an absolute level, as comparable but not exactly the same hardware was used for the TreeQSM

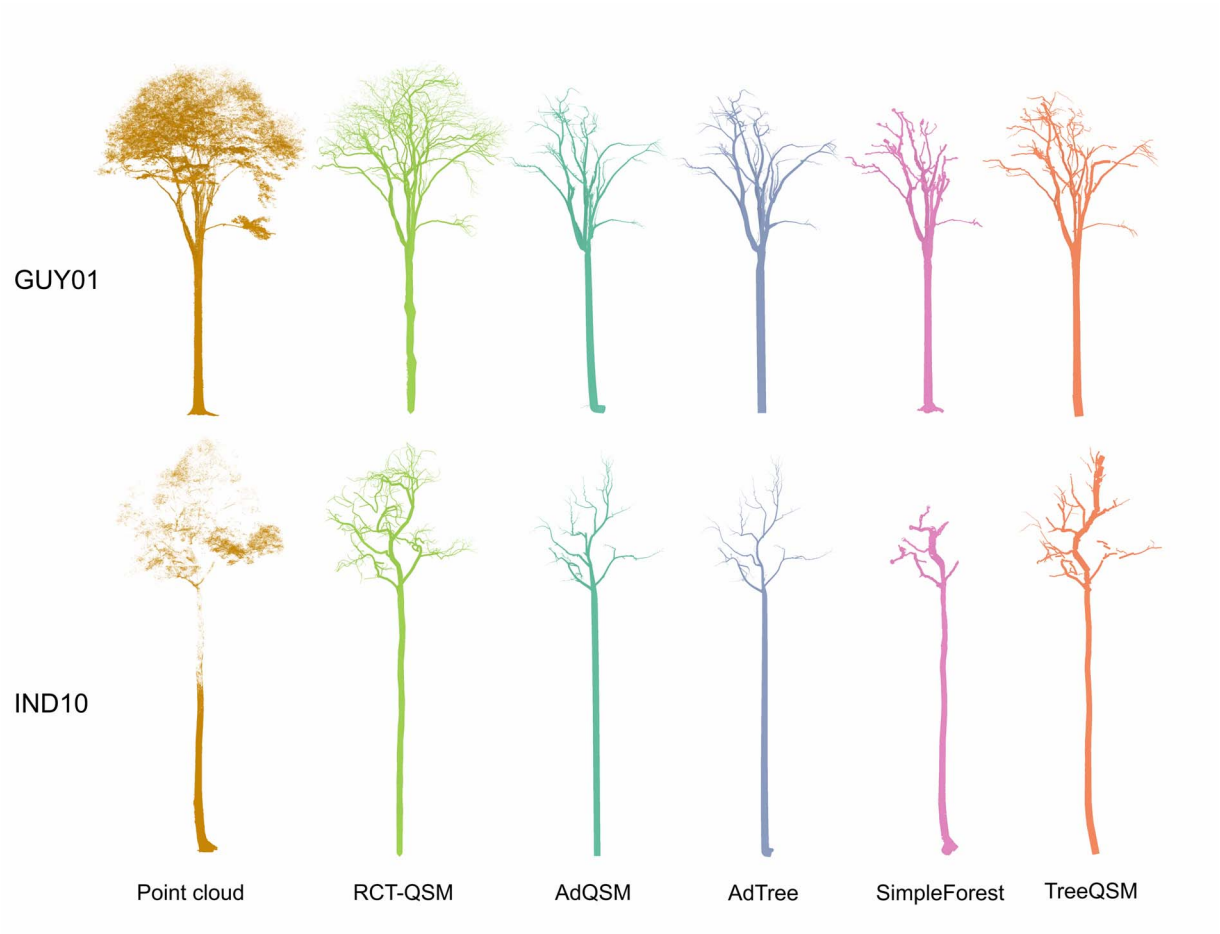

Figure 9. Two exemplary PCs of two trees (GUY01 and IND10) and the corresponding reconstruction results for all tested software tools. For better visibility the results for IND10 were scaled by a factor of 1.5.

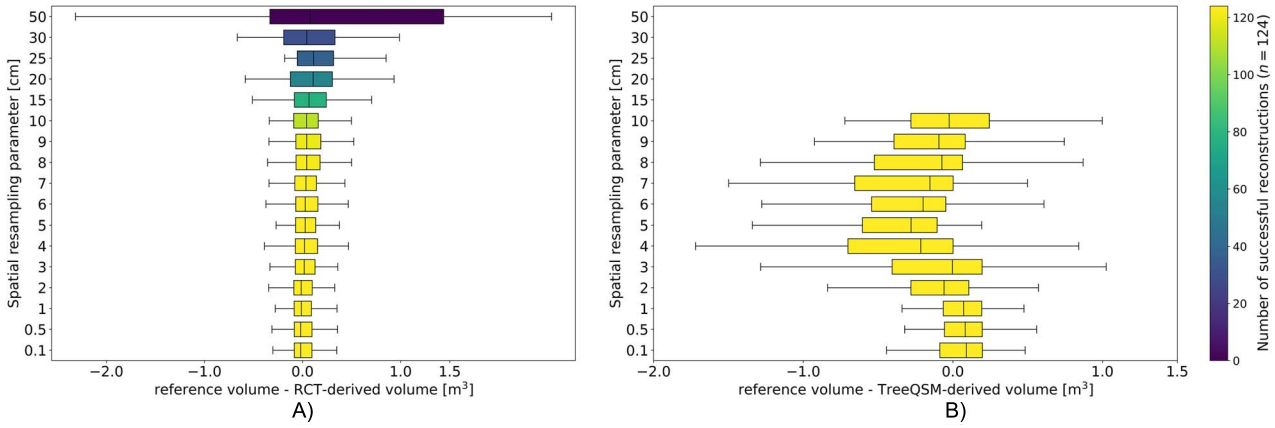

Figure 10. Boxplot diagrams showing the residual volumes of trees from the destructive datasets. Panel (A) presents the residuals for RCTQSM, and panel (B) presents the residuals for TreeQSM. The color of each box indicates the number of PCs that generated a QSM output in RCTQSM and TreeQSM, respectively.

experiments. However, runtimes are at the same order of magnitude.

Scalability and reliability testing

Experimental plot A

Applying the RCT approach to the TLS data from experimental plot A produces the reconstruction shown in Fig. 14. The tree detection and segmentation performance of RCT-QSM was evaluated using a cross-section of both the segmented PC and RCT-QSM generated mesh at ~1.3 m above ground. All 110 trees visible in this cross-section were successfully detected. However, the RCT-QSM struggled with some understory vegetation, such as shrubs and small trees (DBH < 10 cm), which contribute comparatively little to the total biomass and were excluded from analysis. A tent-like branch structure in the plot center (Fig. 2C, far right) also

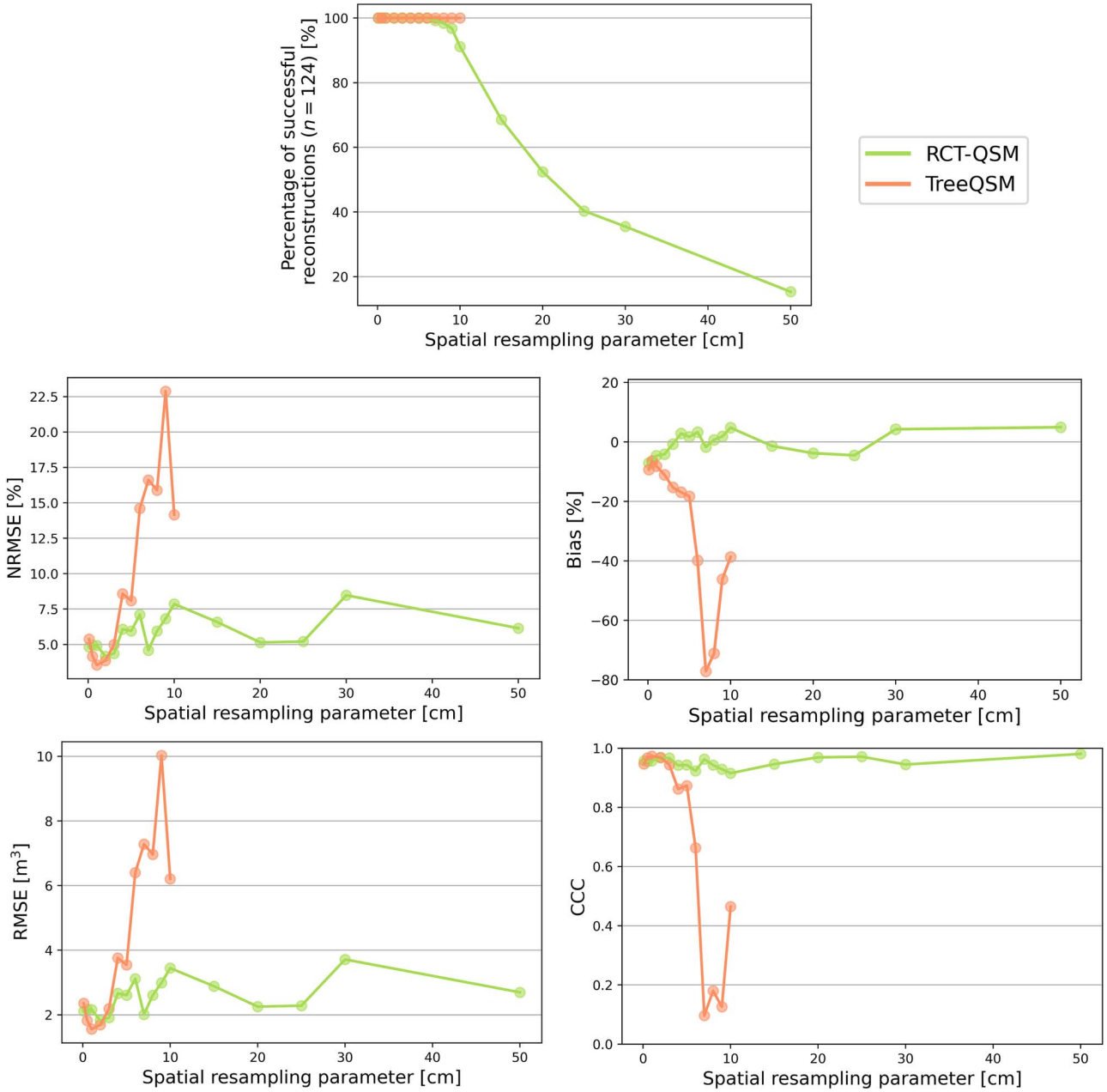

Figure 11. Performance metrics for the various tested resampling parameters. Note that for larger resampling parameters the number of trees decreases as point density decreases (top plot). Consequently, metrics for voxel sizes of 10–50 cm have limited comparability.

produced spurious results in the mesh and was omitted. While further validation is needed, results suggest strong performance in detecting trees and segmenting tree stems. Detailed canopy segmentation analysis, which is more complex due to overlapping crowns, is beyond this paper's scope. However, the close alignment between allometric estimates and RCT-QSM results (see below), and a brief visual inspection suggest good segmentation performance.

There is a generally close alignment between the allometrically and RCT-QSM derived single-tree volumes (CCC = 0.883) with a tendency for overestimation (Bias = 10.2%), which is largely driven by outliers. Three large outliers exhibiting substantial overestimation of volume can be attributed to ivy (*Hedera*) growing along the trees' stems causing a substantial expansion of the 3D mesh (Fig. 15B1). A visual analysis of three larger trees (>20 m in height) reveals a close alignment between the actual branch topology and the RCT-QSM (Fig. 15A1). For these trees, branch and stem diameters also correspond well with the PC. However, deviations are observed in the lower stem regions, where the reconstruction diverges slightly from the PC. This discrepancy is likely due to the reconstruction not fully capturing this part of the tree, as the mesh is extended at a certain height to connect with the terrain, presumably to minimize the influence of spurious ground points caused by potential understory. For the trees in experimental plots A and B, this is likely to have only minimal impact on the estimated volume. However, as mentioned above, for larger tropical trees, this could partially explain the negative bias, as substantial portions of biomass and volume are concentrated in those tree buttresses (Han et al. 2023, Ali et al. 2025).

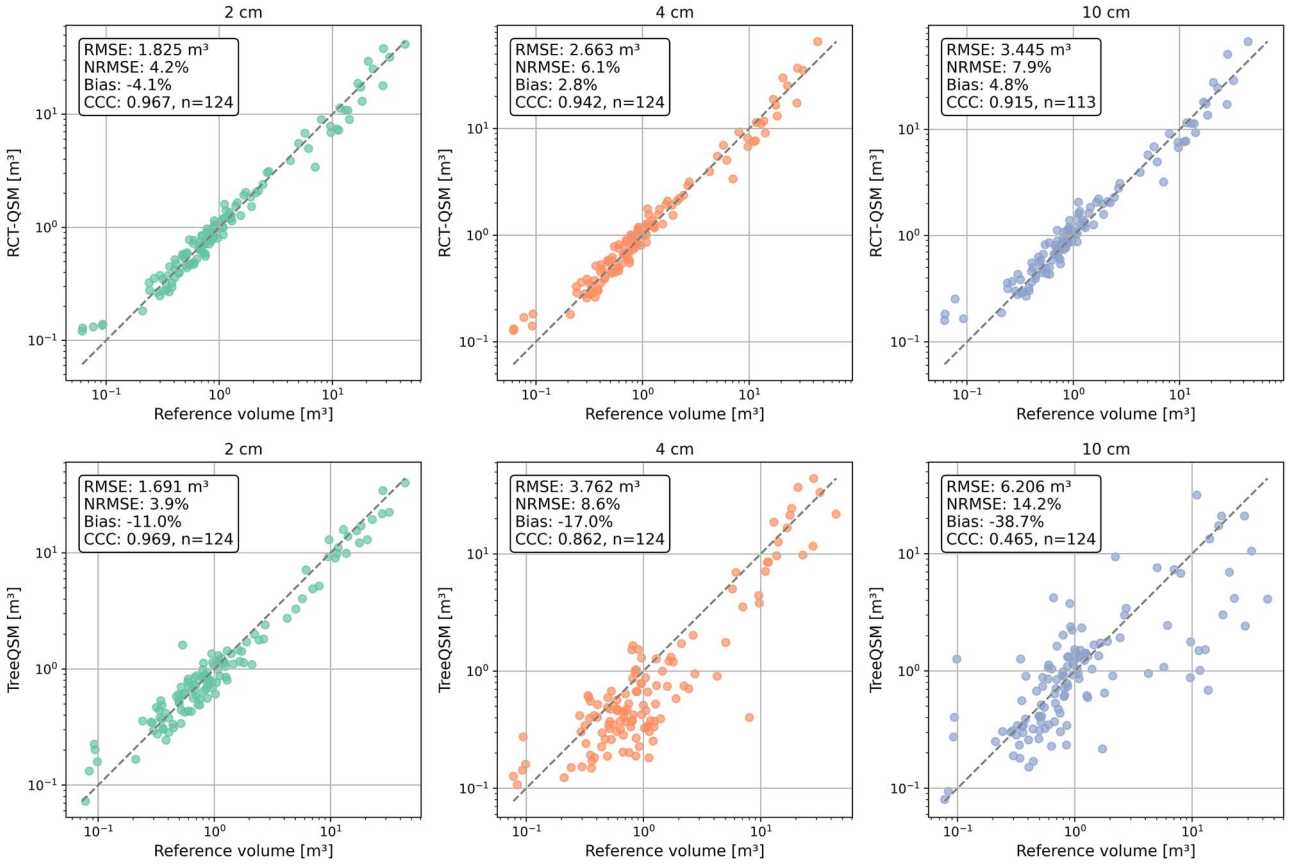

Figure 12. Scatter plots of the RCT-QSM (upper panel) and TreeQSM (lower panel) results from the point sensitivity analysis shown for resampling parameters 2, 4, and 10 cm.

Figure 13. RCT-QSM results from the point sensitivity analysis shown for four resampling parameters (0.1, 5, 10, and 30 cm) for two randomly selected example trees from the destructively harvested dataset: "PSYLB8" from Demol et al. 2021b and "MDD08" from Gonzalez de Tanago et al. (2018).

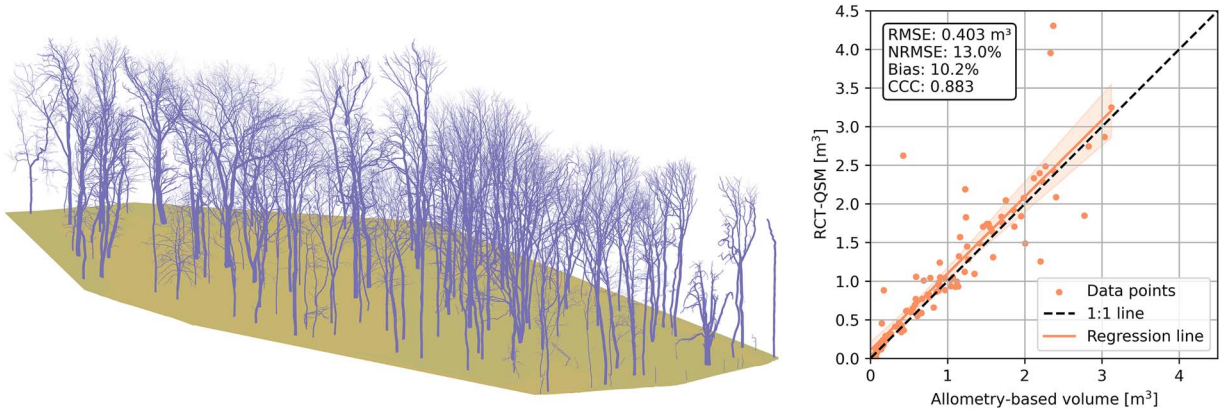

Figure 14. Left: Reconstruction result for experimental plot A displaying the generated ground mesh and the individual QSMs for each tree. Right: Comparison of the RCT-QSM-derived volumes and the allometric volume for experimental plot A. Shaded regions around the linear regression lines represent the 95% confidence intervals of the corresponding regression models.

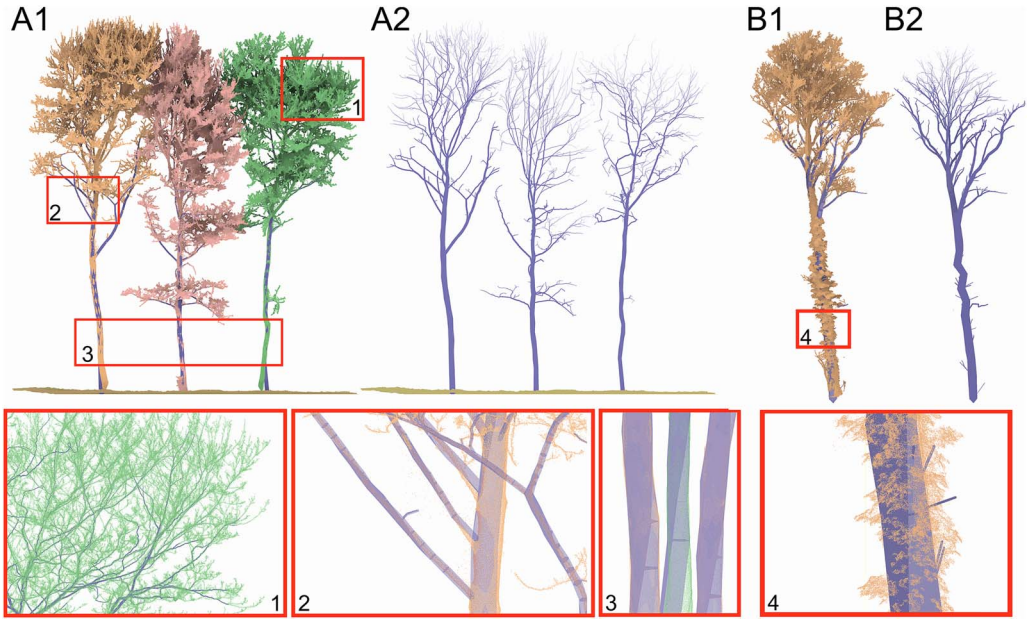

Figure 15. (A1) Segmented and shaded PC and RCT-generated meshes of three trees which are standing next to each other. (B1) Segmented and shaded PC and RCT-generated meshes of a tree featuring extensive ivy growth along the stem. (A2) and (B2) The QSMs of the same trees. The insets 1), 2), 3) and 4) show more detailed depiction of the RCT-generated meshed overlaid with the corresponding PC.

On the machine described in Section 3.3 the two primary processing steps, terrain generation, and PC segmentation with QSM generation, for experimental plot A at its native resolution (8 GB PC with ∼225 million points) required a total of 81 min. This includes 45 min for terrain model derivation and 36 min for segmentation and QSM generation. The maximum memory consumption was 104 GB. However, based on findings from the point density sensitivity analysis, processing times and memory consumption can likely be significantly reduced. Terrain generation was not included in the sensitivity analysis but is expected to remain largely unaffected by variations in point density. It can be expected that even with significantly reduced point counts moderately complex terrains can be reconstructed with reasonable accuracy without adversely affecting QSM generation. Considering the ∼50 min required for scanning at experimental plot A, the entire workflow, excluding travel times but including data management, for estimating single-tree biomass using TLS and RCT-QSM over a ∼3000 m^2 plot takes less than 2 h. However, this does not include any manual intervention, or validity checks, which might be necessary, especially regarding the segmentation results.

Experimental plot B

The dataset for experimental plot B was more challenging. First, occlusions during the acquisition led to significant data gaps along the lower parts of the stem. Second, the reference data are expected to be of inferior quality despite considerable efforts during the manual measurements of DBH and TH. Third, there are strong topographic variations present. Nevertheless, it was possible to obtain RCT-QSMs for all (19) trees for which allometric reference data was obtained and to compare the results (Fig. 16). The results indicate a strong correlation between RCT-QSMs and the allometries (CCC = 0.85). However, the NRMSE (20.6%) for this dataset is significantly higher compared to previously analyzed datasets. Additionally, this plot exhibits a systematic overestimation (26.3%) of RCT-QSM derived volume, likely due to increased noise and reduced point density in the lower sections of the stems.

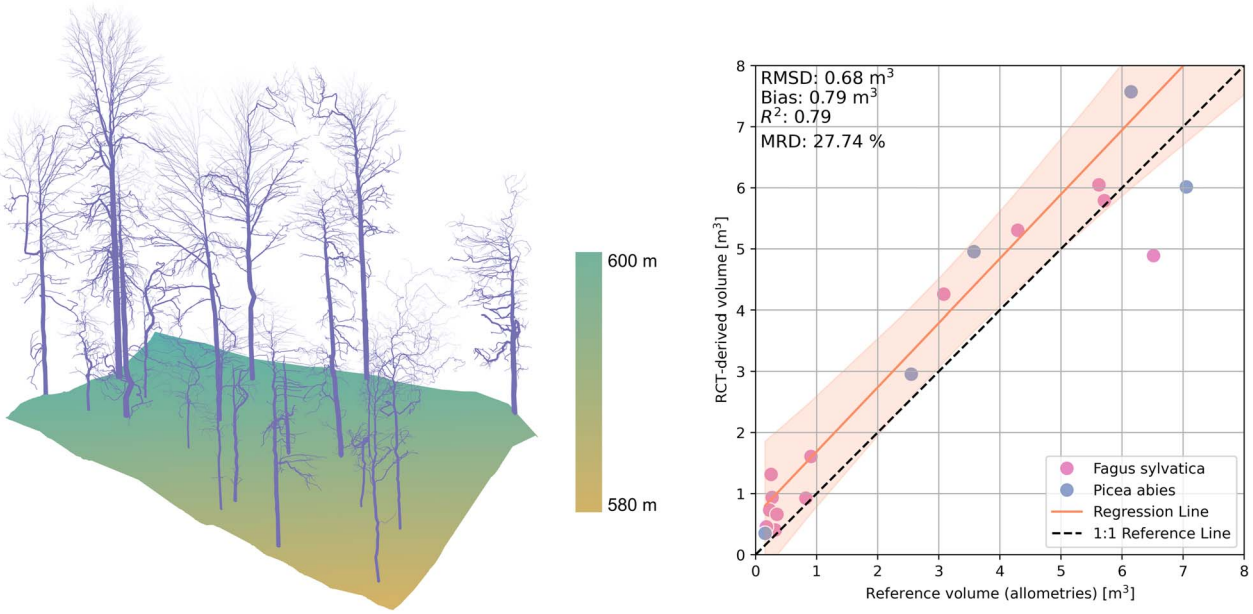

Figure 16. (A1) Segmented and shaded PC and RCT-generated meshes of three trees which are standing next to each other. (B1) Segmented and shaded PC and RCT-generated meshes of a tree featuring extensive ivy growth along the stem. (A2) and (B2) The QSMs of the same trees. The insets 1), 2), 3) and 4) show more detailed depiction of the RCT-generated meshed overlaid with the corresponding PC.

Conclusion

This study provides a comprehensive evaluation of the applicability of RCT-QSM for single-tree volume estimates to enhance AGB estimation in various forest environments, utilizing dynamic UAV-based LS as well as static TLS. The findings are based on various datasets featuring altogether reference volumes and TLS from 124 destructively harvested trees located in seven countries and reference allometry and LS data acquired at two experimental plots in Austria. Compared to destructively harvested single-trees RCT-QSM yields NRMSE of 5% and high CCC of 0.954 with small performance differences between the four reference datasets. It remains to be investigated if these differences arise from tree species, scan protocol, or other sources.

Among the methods evaluated, RCT-QSM and TreeQSM consistently demonstrated the highest accuracy and reliability, with minimal differences in performance. While TreeQSM showed slightly lower (N)RMSE values, RCT-QSM achieved marginally better CCC and smaller bias, clearly outperforming AdQSM, AdTree, and SimpleForest, which exhibited greater errors and substantial biases. Visual and quantitative assessments confirm robust overall performance, though some structural inaccuracies highlight the need for compartment-level validation in future studies.

Reducing point densities up to 1 point per 10 cm voxel only had a marginal influence on the accuracy of the RCT-QSM results indicating robustness against less dense scanning patterns enabling faster data acquisition. As the reduction in point number was spatially uniform, this corresponds to moderate resolution of scans, rather than decreasing the number of scans. The latter could increase the number of occlusions, which does not correspond to a uniform thinning. The impact of occlusions and other PC artifacts on RCT-QSM estimated tree volume remains to be analyzed. Based on the reconstruction success figures and the volatility in metrics, QSM analysis from PCs with density of 1 point per 10 cm voxel or lower is not recommended.

RCT's currently still relatively sparse documentation poses challenges in applying the software and fine-tuning its parameters without examining the source code in detail. Nevertheless, this study demonstrates a very promising performance of RCT-QSM. It performed very well in deriving single-tree volume with high correspondence to destructive data and species-specific allometries. Notably, RCT-QSM allows for a highly automated processing workflow, performing the tree segmentation and 3D modelling in one step. The segmentation results were not explicitly analyzed in this study. However, exemplary validity checks revealed no substantial deviations due to mis-segmentation for the experimental plots, which was also reflected in the generally good agreement with allometries. For more complex plots, the segmentation step could pose greater challenges, as also highlighted by Cherlet et al. (2024). In their segmentation benchmarking (Cherlet et al. 2025), RCT achieved the best performance among all tested segmentation approaches for most plots. Visual inspection showed that larger trees were often split into multiple segments while smaller trees were frequently merged into single instances, leading to missed detections and a lower recall. Regarding the volumetric reconstruction, the results indicate that RCT-QSM outperforms the tested state-of-the-art methods, with the added benefit of more efficient processing of large datasets with minimal parametrization (and no need for single tree segmentation). The point density sensitivity analysis indicates higher robustness against the completeness of the input PC for RCT-QSM, increasing its practicability, e.g. in cases when LS data over larger areas shall be processed.

While RCT-QSM shows promising results in accurately estimating tree volume, a key challenge remains the conversion of single-tree volume to AGB. This conversion is challenging due to the significant variability of wood density among species, across biomes, and even within individual trees. Accurate AGB estimation requires multiplying single-tree volume by basic wood density, which is the ratio of oven-dry mass to green volume. However, these conversions introduce substantial uncertainties. Wood density can vary significantly between trees of the same species and even within individual trees, as demonstrated by

Burt et al. (2021), who observed large gradients in tissue density within individuals growing on different substrates and across THs. LS cannot provide information about tree-specific wood density. In the absence of tree-specific data, databases like the GWDD (Chave et al. 2009, Zanne et al. 2009) provide tabulated species-specific wood densities, a practical but imperfect solution, introducing uncertainties of up to 10% (Demol et al. 2021a). This variability highlights that even with rigorous efforts to reduce measurement uncertainty, derived AGB values may still deviate from actual AGB.

Taken together, these uncertainties underscore the need for improved, scalable approaches to tree-level volume estimation, an area in which RCT-QSM shows considerable promise. RCT-QSM can greatly improve the automation and efficiency of deriving single-tree volumes, thereby significantly automating the process of identifying species-specific allometries. This could also benefit communities that lack access to or expertise in utilizing LS and RCT-QSM. However, given the novelty of RCT-QSM and the limited number of studies utilizing this tool, more experience needs to be gathered and shared among potential users of RCT-QSM. In particular, the processing parameters of RCT-QSM and its performance across different tree compartments would deserve further exploration in future studies. Also, its applicability in more challenging environments and scenarios with less dense and dynamic scanning patterns needs to be evaluated. Our findings suggest that RCT-QSM is a highly competitive and efficient tool for generating high-quality single-tree volume estimates at large scales with minimal parameterization.

Ground-based LS, whether from static or dynamic platforms (TLS, MLS), was demonstrated to deliver valuable information for forest inventories (Liang et al. 2016). Also, national forest inventory (NFI) authorities are investigating these possibilities and constraints (Holvoet et al. 2025). The high reliability of generating QSMs with RCT, that we have found in our study, suggests their use for obtaining very accurate tree volume for entire NFI plots. The reliability applies to both, single tree volume and performance at plot level. Together with additional information on tree species and their corresponding wood density this could establish QSMs as the source of AGB in any forest inventory, moving from a field-estimate based on allometric equations to a "measurement". The practicability of QSMs might also open an interesting avenue to obtain merchantable wood volume and advance forest economy. As with many technical advancements in forestry, a major challenge will be the practical implementation into practitioners' workflows. To address this, efforts will be needed to lower the entry barriers and ensure these tools can be used effectively. Following the verification of reliability and accuracy, efficiency, especially with respect to data acquisition for QSMs, will have to be investigated next. With high density PCs from high-quality UAV-borne LS, single tree QSMs for entire forest transects or for larger plots become an option [as investigated in Bohn Reckziegel et al. (2025) for savanna/open forest]. This will allow increasing the number of reference and training data and reducing the necessary extrapolation for assessing wood volume for large forest areas.

Acknowledgements

The authors acknowledge the TU Wien Bibliothek for financial support through its Open Access Funding Programme.

Author contributions

Benjamin Wild (Conceptualization, Methodology, Investigation, Validation, Software, Formal Analysis, Data Curation, Writing—Original Draft), Taskin Özkan (Conceptualization, Software, Investigation, Methodology, Writing—review & editing), Moonis Ali (Data Curation, Writing—review & editing), Florian Pöppl (Conceptualization, Software, Writing—review & editing), Milutin Milenkovic (Funding acquisition, Writing—review & editing), Florian Hofhansl (Writing—review & editing), Norbert Pfeifer (Supervision, Writing—review & editing), Alvaro Lau (Data curation, Writing—review & editing), and Markus Hollaus (Conceptualization, Funding acquisition, Supervision, Writing—review & editing)

Conflict of interest

None declared.

Funding

This work is part of the project "Citizens for Copernicus (C4C): Combing Copernicus and Crowdsource Data for Forest Resources Monitoring" funded by the Austrian Research Promotion Agency (FFG) under the ASAP 2022 call, Application ID: https://projekte.ffg.at/projekt/4712922.

Software and data availability statement

The table below provides a summary of the availability of the destructive datasets utilized in this study (information current as of 27 November 2024).

Reference	Type	License	DOI
Demol et al. (2021c)	TLS and destructive data	CC BY 4.0	https://doi.org/10.5281/zenodo.4557401
Hackenberg (2021)	TLS and destructive data	CC BY 4.0	https://doi.org/10.5281/zenodo.5131717
Gonzales de Tanago et al. (2022)	TLS and destructive data	CCBY4.0	https://doi.org/10.4121/21552084.v1

The RCT software can be downloaded from Github (Lowe and Stepanas 2021): https://github.com/csiro-robotics/raycloudtools

The QSM reconstruction of TreeQSM, AdQSM, AdTree, and SimpleForest were provided by Ali et al. (2025).

The other data that support the findings of this study are available upon reasonable request, including the TreeQSM models for different point density, which were provided by Moonis Ali.

Declaration of generative AI and AI-assisted technologies in the writing process

During the preparation of this work the authors used ChatGPT (GPT-4o and GPT-4o mini) to improve the readability and language of the manuscript. After using this tool, the authors reviewed and edited the content as needed and take full responsibility for the content of the published article.

References

Abegg M, Bösch R, Kükenbrink D *et al.* Tree volume estimation with terrestrial laser scanning—testing for bias in a 3D virtual environment. *Agric For Meteorol* 2023;**331**:109348. https://doi.org/10.1016/J.AGRFORMET.2023.109348.

Ali M, Lohani B, Hollaus M *et al.* A hybrid approach for enhanced tree volume estimation of complex trees using terrestrial LiDAR. *GIScience Remote Sens* 2025;**62**:2474836. https://doi.org/10.1080/15481603.2025.2474836.

Arseniou G, MacFarlane DW, Calders K *et al.* Accuracy differences in aboveground woody biomass estimation with terrestrial laser scanning for trees in urban and rural forests and different leaf conditions. *Trees* 2023;**37**:761–79. https://doi.org/10.1007/s00468-022-02382-1.

Belete Y, Abere F, Kebede B *et al.* Nondestructive allometric model to estimate aboveground biomass: An alternative approach to generic pan-tropical models. *Sch Res Libr J Nat Prod Plant Resour* 2021;**11**:1–10.

Bickelhaupt DH, Leaf AL, Richards NA. Effect of branching habit on aboveground dry weight estimates of Acer saccharum stands. In: Young HE, (ed.). *IUFRO Biomass Studies: Nancy, France, and Vancouver, B.C., Canada*. Orono, Maine: University of Maine, College of Life Sciences and Agriculture, 1973, 219–30.

Bohn Reckziegel R, Lowe T, Devereux T *et al.* Assessing the reliability of woody vegetation structural characterisation from UAV-LS in a tropical savanna. *Sci Remote Sens* 2025;**11**:100178. https://doi.org/10.1016/J.SRS.2024.100178.

Brede B, Calders K, Lau A *et al.* Non-destructive tree volume estimation through quantitative structure modelling: Comparing UAV laser scanning with terrestrial LIDAR. *Remote Sens Environ* 2019;**233**:111355. https://doi.org/10.1016/J.RSE.2019.111355.

Brenneman BB, Frederick DJ, Gardner WE *et al.* Biomass of species and stands of West Virginia hardwoods. In: Pope PE, (ed.). *Proceedings of Central Hardwood Forest Conference II*. West Lafayette: Purdue University, 1978, 159–78.

Burt A, Boni Vicari M, Da Costa ACL *et al.* New insights into large tropical tree mass and structure from direct harvest and terrestrial lidar. *R Soc Open Sci* 2021;**8**:201458. https://doi.org/10.1098/RSOS.201458.

Calders K, Adams J, Armston J *et al.* Terrestrial laser scanning in forest ecology: Expanding the horizon. *Remote Sens Environ* 2020;**251**:112102. https://doi.org/10.1016/J.RSE.2020.112102.

Chave J, Andalo C, Brown S *et al.* Tree allometry and improved estimation of carbon stocks and balance in tropical forests. *Oecologia* 2005;**145**:87–99. https://doi.org/10.1007/s00442-005-0100-x.

Chave J, Coomes D, Jansen S *et al.* Towards a worldwide wood economics spectrum. *Ecol Lett* 2009;**12**:351–66. https://doi.org/10.1111/J.1461-0248.2009.01285.X.

Cherlet W, Cooper Z, Van Den Broeck WAJ *et al.* Benchmarking instance segmentation in terrestrial laser scanning Forest point clouds. In: *IGARSS 2024–2024 IEEE International Geoscience and Remote Sensing Symposium*, Athens, Greece, 7–12 July 2024; pp. 4511–4515. https://doi.org/10.1109/IGARSS53475.2024.10642025.

Cherlet W, Cooper Z, Van den Broeck WAJ *et al.* Benchmarking tree instance segmentation of terrestrial laser scanning for biomass estimation. *Remote Sens Environ* 2025;**231**:230–247:S0924-2716(25)00423-X.

Chopping M, Wang Z, Schaaf C *et al.* Forest aboveground biomass in the southwestern United States from a MISR multi-angle index, 2000–2015. *Remote Sens Environ* 2022;**275**:112964. https://doi.org/10.1016/J.RSE.2022.112964.

Dalla Corte AP, de Vasconcellos BN, Rex FE *et al.* Applying high-resolution UAV-LiDAR and quantitative structure modelling for estimating tree attributes in a crop-livestock-Forest system. *Land (Basel)* 2022;**11**:507. https://doi.org/10.3390/land11040507.

Demol M, Calders K, Krishna Moorthy SM *et al.* Consequences of vertical basic wood density variation on the estimation of aboveground biomass with terrestrial laser scanning. *Trees* 2021a;**35**:671–84. https://doi.org/10.1007/s00468-020-02067-7.

Demol M, Calders K, Verbeeck H *et al.* Forest above-ground volume assessments with terrestrial laser scanning: A ground-truth validation experiment in temperate, managed forests. *Ann Bot* 2021b;**128**:805–19. https://doi.org/10.1093/AOB/MCAB110.

Demol M, Gielen B, Verbeeck H. *QSMs, Point Cloud and Harvest Data from a Destructive Forest Biomass Experiment in Belgium Using Terrestrial Laser Scanning*, Zenodo, 2021c. https://doi.org/10.5281/zenodo.4557401.

Demol M, Verbeeck H, Gielen B *et al.* Estimating forest above-ground biomass with terrestrial laser scanning: Current status and future directions. *Methods Ecol Evol* 2022a;**13**:1628–39. https://doi.org/10.1111/2041-210X.13906.

Demol M, Wilkes P, Raumonen P *et al.* Volumetric overestimation of small branches in 3D reconstructions of Fraxinus excelsior. *Silva Fenn* 2022b;**56**:10550. https://doi.org/10.14214/SF.10550.

Disney M, Burt A, Wilkes P *et al.* New 3D measurements of large redwood trees for biomass and structure. *Sci Rep* 2020;**10**:16721. https://doi.org/10.1038/s41598-020-73733-6.

Du S, Lindenbergh R, Ledoux H *et al.* AdTree: Accurate, detailed, and automatic modelling of laser-scanned trees. *Remote Sens* 2019;**11**:2074. https://doi.org/10.3390/RS11182074.

Dutcă I. The variation driven by differences between species and between sites in allometric biomass models. *Forests* 2019;**10**:976. https://doi.org/10.3390/F10110976.

Fan G, Nan L, Dong Y *et al.* AdQSM: A new method for estimating above-ground biomass from TLS point clouds. *Remote Sens* 2020;**12**:3089. https://doi.org/10.3390/RS12183089.

Freedman B, Duinker PN, Barclay H *et al. Forest Biomass and Nutrient Studies in Central Nova Scotia*, For. Ecol. Manage, 1982.

Fremout T, Cobián-De Vinatea J, Thomas E *et al.* Site-specific scaling of remote sensing-based estimates of woody cover and above-ground biomass for mapping long-term tropical dry forest degradation status. *Remote Sens Environ* 2022;**276**:113040. https://doi.org/10.1016/J.RSE.2022.113040.

Girardeau D. *CloudCompare (Version 2.13.0) [GPL Software]*, 2024.

Gonzales J, Lau Sarmiento A, Bartholomeus H *et al. Data Underlying the Publication: Estimation of above-Ground Biomass of Large Tropical Trees with Terrestrial LiDAR*, 2022. https://doi.org/10.4121/21552084.v1.

Gonzalez de Tanago J, Lau A, Bartholomeus H *et al.* Estimation of above-ground biomass of large tropical trees with terrestrial LiDAR. *Methods Ecol Evol* 2018;**9**:223–34. https://doi.org/10.1111/2041-210X.12904.

Grabherr G, Peter C, Enzenhofer J *et al. Ein Wald Im Aufbruch: das Naturwaldreservat Rohrach (Vorarlberg, Österreich), Bristol-Schriftenreihe*. Teufen: Flück-Wirth, 1999.

Hackenberg, J. 2021. Hackenberg et al 2021. https://doi.org/10.5281/zenodo.5131717.

Hackenberg J, Spiecker H, Calders K *et al.* SimpleTree —An efficient open source tool to build tree models from TLS clouds. *Forests* 2015a;**6**:4245–94. https://doi.org/10.3390/f6114245.

Hackenberg J, Wassenberg M, Spiecker H *et al.* Non destructive method for biomass prediction combining TLS derived tree volume and wood density. *Forests* 2015b;**6**:1274–300. https://doi.org/10.3390/f6041274.

Han T, Raumonen P, Sánchez-Azofeifa GA. A non-destructive approach to estimate buttress volume using 3D point cloud data. *Eco Inform* 2023;**77**:102218. https://doi.org/10.1016/j.ecoinf.2023.102218.

Henry M, Bombelli A, Trotta C *et al.* GlobAllomeTree: International platform for tree allometric equations to support volume, biomass and carbon assessment. *IForest* 2013;**6**:326. https://doi.org/10.3832/IFOR0901-006.

Hirata Y, Tabuchi R, Patanaponpaiboon P *et al.* Estimation of aboveground biomass in mangrove forests using high-resolution satellite data. *J For Res* 2014;**19**:34–41. https://doi.org/10.1007/S10310-013-0402-5/FIGURES/7.

Holvoet J, Eichhorn MP, Giannetti F *et al.* Terrestrial and mobile laser scanning for national forest inventories: From theory to implementation. *Remote Sens Environ* 2025;**329**:114947. https://doi.org/10.1016/j.rse.2025.114947.

Hu T, Su Y, Xue B *et al.* Mapping global Forest aboveground biomass with spaceborne LiDAR, optical imagery, and Forest inventory data. *Remote Sens* 2016;**8**:565. https://doi.org/10.3390/RS8070565.

Huang X, Ziniti B, Torbick N *et al.* Assessment of Forest above ground biomass estimation using multi-temporal C-band Sentinel-1 and polarimetric L-band PALSAR-2 data. *Remote Sens* 2018;**10**:1424. https://doi.org/10.3390/RS10091424.

Katz S, Tal A. On the visibility of point clouds. *IEEE International Conference on Computer Vision (ICCV)*, Santiago, Chile, 2015, pp. 1350–1358. https://doi.org/10.1109/ICCV.2015.159.

Ker MF. *Tree Biomass Equations for Seven Species in Southwestern New Brunswick*, Maritimes Forest Research Centre, New Brunswick 1980.

Kükenbrink D, Gardi O, Morsdorf F *et al.* Above-ground biomass references for urban trees from terrestrial laser scanning data. *Ann Bot* 2021;**128**:709–24. https://doi.org/10.1093/AOB/MCAB002.

Laino D, Cabo C, Prendes C *et al.* 3DFin: A software for automated 3D forest inventories from terrestrial point clouds. *Forestry Int J For Res* 2024;**97**:cpae020. https://doi.org/10.1093/forestry/cpae020.

Lau A, Bentley LP, Martius C *et al.* Quantifying branch architecture of tropical trees using terrestrial LiDAR and 3D modelling. *Trees-Struct Funct* 2018;**32**:1219–31. https://doi.org/10.1007/S00468-018-1704-1/FIGURES/4.

Le Toan T, Quegan S, Davidson MWJ *et al.* The BIOMASS mission: Mapping global forest biomass to better understand the terrestrial carbon cycle. *Remote Sens Environ* 2011;**115**:2850–60. https://doi.org/10.1016/J.RSE.2011.03.020.

Liang X, Kankare V, Hyyppä J *et al.* Terrestrial laser scanning in forest inventories. *ISPRS J Photogramm Remote Sens* 2016;**115**:63–77. https://doi.org/10.1016/j.isprsjprs.2016.01.006.

Lin LI-K. A concordance correlation coefficient to evaluate reproducibility. *Biometrics* 1989;**45**:255–68. https://doi.org/10.2307/2532051.

Lowe T, Moghadam P, Edwards E *et al.* Canopy density estimation in perennial horticulture crops using 3D spinning lidar SLAM. *J Field Robot* 2021;**38**:598–618. https://doi.org/10.1002/rob.22006.

Lowe T, Stepanas K. RayCloudTools: A concise Interface for analysis and manipulation of ray clouds. *IEEE Access* 2021;**9**:79712–24. https://doi.org/10.1109/ACCESS.2021.3084954.

Malhi Y, Jackson T, Bentley LP *et al.* New perspectives on the ecology of tree structure and tree communities through terrestrial laser scanning. *Interface Focus* 2018;**8**:20170052. https://doi.org/10.1098/RSFS.2017.0052.

Momo Takoudjou S, Ploton P, Sonké B *et al.* Using terrestrial laser scanning data to estimate large tropical trees biomass and calibrate allometric models: A comparison with traditional destructive approach. *Methods Ecol Evol* 2018;**9**:905–16. https://doi.org/10.1111/2041-210X.12933.

Morhart C, Schindler Z, Frey J *et al.* Limitations of estimating branch volume from terrestrial laser scanning. *Eur J For Res* 2024;**143**:687–702. https://doi.org/10.1007/S10342-023-01651-Z/TABLES/3.

Muntoni A, Cignoni P. *PyMeshLab*, Zenodo, 2021. https://doi.org/10.5281/zenodo.4438750.

Ogle SM, Kurz WA, Green C *et al.* Chapter 2 generic methodologies applicable to multiple land-use categories. In: *Refinement to the 2006 IPCC Guidelines for National Greenhouse Gas Inventories*, IPCC, 2019.

Pastor J, Bockheim JG. Biomass and production of an aspen-mixed hardwood-spodosol ecosystem in northern Wisconsin. *Can J For Res* 1981;**11**:132–8.

Perala DA, Alban DH. *Allometric Biomass Estimators for Aspen-Dominated Ecosystems in the Upper Great Lakes*, St. Paul, MN: U.S. Dept. of Agriculture, Forest Service, North Central Forest Experiment Station, 1994.

Pfeifer N, Mandlburger G, Otepka J *et al.* OPALS – A framework for airborne laser scanning data analysis. *Comput Environ Urban Syst* 2014;**45**:125–36. https://doi.org/10.1016/J.COMPENVURBSYS.2013.11.002.

Raumonen P, Kaasalainen M, Markku Å *et al.* Fast automatic precision tree models from terrestrial laser scanner data. *Remote Sens* 2013;**5**:491–520. https://doi.org/10.3390/RS5020491.

Saarela S, Wästlund A, Holmström E *et al.* Mapping aboveground biomass and its prediction uncertainty using LiDAR and field data, accounting for tree-level allometric and LiDAR model errors. *For Ecosyst* 2020;**7**:43. https://doi.org/10.1186/s40663-020-00245-0.

Schieler K. *Methodische Fragen in Zusammenhang Mit der Österreichischen Forstinventur*, Universität für Bodenkultur, Wien, 1988.

Schmidt L, Forkel M, Zotta RM *et al.* Assessing the sensitivity of multi-frequency passive microwave vegetation optical depth to vegetation properties. *Biogeosciences* 2023;**20**:1027–46. https://doi.org/10.5194/BG-20-1027-2023.

Stovall AEL, Shugart HH, Stovall AEL *et al.* Assessing terrestrial laser scanning for developing non-destructive biomass allometry. *For Ecol Manag* 2018;**427**:217–29. https://doi.org/10.1016/J.FORECO.2018.06.004.

Swenson NG, Enquist BJ. Ecological and evolutionary determinants of a key plant functional trait: Wood density and its community-wide variation across latitude and elevation. *Am J Bot* 2007;**94**:451–9. https://doi.org/10.3732/AJB.94.3.451.

Ter-Mikaelian MT, Korzukhin MD. Biomass equations for sixty-five north American tree species. *For Ecol Manag* 1997;**97**:1–24. https://doi.org/10.1016/S0378-1127(97)00019-4.

Teubner IE, Forkel M, Wild B *et al.* Impact of temperature and water availability on microwave-derived gross primary production. *Biogeosciences* 2021;**18**:3285–308. https://doi.org/10.5194/bg-18-3285-2021.

Tian L, Wu X, Tao Y *et al.* Review of remote sensing-based methods for Forest aboveground biomass estimation: Progress, challenges, and prospects. *Forests* 2023;**14**:1086. https://doi.org/10.3390/F14061086.

Whittaker RH, Bormann FH, Likens GE *et al.* The Hubbard brook ecosystem: Forest biomass and production. *Ecol Monogr* 1974;**44**:233–52.

World Meteorological Organization (WMO), United Nations Environment Programme (UNEP), International Science Council (ISC), Intergovernmental Oceanographic Commission of the

United Nations Educational, S. and C.O. IOC-U. *GCOS 2022 Implementation Plan*, World Meteorological Organization (WMO), 2022.

Ye N, van Leeuwen L, Nyktas P. Analysing the potential of UAV point cloud as input in quantitative structure modelling for assessment of woody biomass of single trees. *Int J Appl Earth Obs Geoinf* 2019;**81**:47–57. https://doi.org/10.1016/J.JAG.2019.05.010.

Young HE, Ribe JH, Wainwright K. *Weight Tables for Tree and Shrub Species in Maine*, Life Sciences and Agriculture Experiment Station, Orono, 1980.

Zanne AE, Lopez-Gonzalez G, Coomes DA *et al. Data from: Towards a Worldwide Wood Economics Spectrum*, Dryad, 2009. https://doi.org/10.5061/dryad.234.

Zianis D, Muukkonen P, Mäkipää R *et al.* Biomass and stem volume equations for tree species in Europe. *Silva Fenn Monographs* 2005;**4**:1–63. https://doi.org/10.14214/SF.SFM4.

Zotta R-M, Moesinger L, van der Schalie R *et al.* VODCA v2: Multi-sensor, multi-frequency vegetation optical depth data for long-term canopy dynamics and biomass monitoring. *Earth Syst Sci Data Discuss* 2024;**2024**:1–45. https://doi.org/10.5194/essd-2024-35.

Forestry: An International Journal of Forest Research, 2026, **99**, 1–20
https://doi.org/10.1093/forestry/cpaf087
Original Article